CFD Letters

Journal homepage:
https://semarakilmu.com.my/journals/index.php/CFD_Letters/index
ISSN: 2180-1363

Base Pressure Control using Quarter Circle Rib in a Suddenly Expanded Duct at Screech Prone Mach Number M = 1.8

Zakir Ilahi Chaudhary[1], Ambareen Khan[2], Sher Afghan Khan[3,*], Khizar Ahmed Pathan[4]

[1] Department of Mechanical Engineering Automobile, M. H. Saboo Siddik College of Engineering, Mumbai 400008, India
[2] Centre for Instructional Technology and Multimedia, Universiti Sains Malaysia, Pulau Pinang, Malaysia
[3] Department of Mechanical & Aerospace Engineering, Faculty of Engineering, International Islamic University Malaysia, Gombak, 53100 Kuala Lumpur, Malaysia
[4] Department of Mechanical Engineering, CSMSS Chh. Shahu College of Engineering, Aurangabad, Maharashtra 431001, India

ARTICLE INFO

Article history:
Received 2 December 2024
Received in revised form 29 December 2024
Accepted 20 January 2025
Available online 28 February 2025

Keywords:
Base drag; screech prone Mach number; L/D ratio; level of expansion

ABSTRACT

Occurrence of sudden expansion is widespread in the defence and automobile industry. At the blunt base of the fuselage, missiles, projectiles and aircraft bombs, the flow gets separated at the base and forms low-pressure recirculation, leading to a significant increase in the base drag. This paper addresses how this low base pressure at the base can be controlled. In this study, quarter circle ribs are used as a control mechanism to regulate the base pressure in a suddenly expanded flow of area ratio 4.84, Mach M = 1.8 for nozzle pressure ratios (NPRs) ranging from 3 to 11 at various rib locations in the range from 11 mm, 22mm, 33 mm, 44 mm and 66mm for duct length ranging from L = 1D to 6D. Results show for 11 mm rib location and 1 mm rib radius, there is a declining trend in the base till nozzle pressure ratio of 6 and for further increases in the expansion level, there is a progressive increase in the base pressure ratio. The highest base pressure value is 2 for a 4 mm rib radius at the highest simulated nozzle pressure ratio. This trend continues for 22 mm rib locations. With a further shift in the rib location, there is a considerable increase in the base pressure ratio. These values are 2.5, 3 and 3.75 for rib locations at 33 mm, 44 mm and 66 mm for a rib radius of 4 mm at the highest level of under-expansion. It is seen that even though the effectiveness of the 1 mm rib radius was nil for all the rib locations except when the rib is located at 66 mm. When a quarter circle rib of radius 1 mm is used, there is a significant increase in the base pressure and base suction is nearly zero. This study is a technology demonstration and the database created from this study can be used to design aerospace vehicles. It will be beneficial at the initial design stage as a wind tunnel test is costly.

1. Introduction

Turbulence has been an enigma since the beginning of fluid science. Since we cannot avoid turbulence in the natural and engineered flows surrounding us, we must understand it. Understanding turbulence is necessary to control the drag associated with turbulent flows. When fluids are mixed or an increase in skin friction drag is required, there are flows where turbulence is

* *Corresponding author.*
E-mail address: sakhan@iium.edu.my (Sher Afghan Khan)

https://doi.org/10.37934/cfdl.17.8.6095

desired. In engineering flows, however, turbulence is undesirable and should be controlled to minimize energy input. Significant financial and ecological consequences are linked to turbulent drag in engineering and real-world flows. The use of fossil fuels by various processes

In the subsonic and supersonic regimes, sudden flow expansion is a significant problem with numerous applications. Utilizing a jet and shroud combination as a supersonic parallel diffuser is an excellent application of unanticipated expansion issues. Another exciting application is a jet that discharges into a shroud and creates a suitable sub-atmospheric discharge pressure; this system is found in the system that simulates high altitude conditions in test cells for jet and rocket engines. When hot exhaust gas jets stream past the exhaust valve, similar flow conditions exist in an internal combustion engine's exhaust port. The flow around the base of a projectile or missile in flight with a blunt edge provides another relevant example; in this instance, the flow extends inward rather than outward, like in the previous example.

Utilizing a supersonic jet and shroud arrangement in conjunction with the sudden flow expansion in both the subsonic and supersonic domains poses a significant challenge for numerous applications. Utilizing a parallel diffuser is an excellent method for handling abrupt expansion difficulties. A further intriguing use is in the system that simulates high-altitude environments in test cells for rockets and aircraft engines. This system produces a sufficient sub-atmospheric discharge pressure when a jet discharges into a shroud. The flow condition of an exhaust valve that allows a stream of hot exhaust gases to pass through is comparable to that of an internal combustion engine's exhaust port. When a projectile or missile with blunt edges is in flight, the flow around its base flows inward rather than outward, as in the previous case, providing another pertinent illustration.

Flow separation, recirculation and reattachment define the intricate phenomenon known as the abrupt axisymmetric expansion flowfield. A dividing streamline or dividing surface, can split such a flowfield into two core parts: the central flow region and the flow recirculation region. The reattachment point is where the dividing streamline strikes the wall.

Hence, this study is undertaken to regulate the base pressure using quarter ribs of various radii, rib locations ranging from 11 mm to 66 mm for NPRs ranging from 3 to 11 and duct lengths in the range from 22 mm to 132 mm at Mach M = 1.8 which is a screech prone Mach number. And to the best of the author's knowledge, no study has been done using quarter rib as a passive control mechanism to regulate the base pressure at high Mach numbers like M = 1.8

2. Literature Review

In this section, we will scan the literature on the base pressure control in a suddenly expanded flow. There are two methods of control:

i. Passive control
ii. Active control.

Passive control can be accomplished by altering the geometry whenever the active control mechanism is used. It requires an external source of energy, which is very complex if the same is not available through the propulsion system of the aerospace system.

Pathan *et al.,* [1] and Fiqri *et al.,* [2] underscored the significance of optimizing expansion geometry to improve base flow characteristics; this highlights the pivotal role of design in augmenting aerodynamic efficiency. Similarly, Aqilah *et al.,* [3] and Pathan *et al.,* [4] examined control mechanisms in flows characterized by sudden expansions and cavities at sonic Mach numbers. They discovered that strategically positioned cavities effectively facilitated flow reattachment and

elevated base pressure, demonstrating their utility as passive control strategies. Furthermore, Pathan *et al.,* [5] and Azami *et al.,* [6] investigated the influence of duct length on flow management, revealing its critical importance in minimizing pressure losses and enhancing performance in expanded flows. However, these findings collectively elucidate the intricate relationship between design parameters and aerodynamic behaviour, suggesting that, although challenges persist, significant advancements are attainable through targeted research and innovative methodologies.

Pathan *et al.,* [7] conducted a comprehensive analysis of supersonic flow dynamics within converging-diverging nozzles, ultimately concluding that nozzle configurations significantly influence flow patterns; this insight aids in developing passive control techniques. Furthermore, subsequent investigations by Azami *et al.,* [8] revealed that the optimization of nozzle design, particularly concerning wall thickness variations, substantially enhances performance and mitigates structural weight, thereby providing distinct advantages for aerospace applications. Recent work underscores the critical importance of both passive and active control techniques in optimizing high-speed aerodynamic configurations [9-11]. Passive strategies, especially those involving optimized geometries, consistently demonstrate improvements in efficiency without necessitating active interventions [12-16]. However, integrating advanced methodologies, such as Computational Fluid Dynamics (CFD), presents formidable challenges because of the inherent complexity associated with fluid dynamics [17-20]. Computational Fluid Dynamics (CFD) has become a cornerstone in many applications. Chaudhari *et al.,* [21] underscored its significance in elucidating combustion strategies within catalytic converter; however, Jain *et al.,* [22] illustrated the influence of heat sink orientation on thermal performance, emphasizing the necessity of geometric optimization.

Furthermore, Shaikh *et al.,* [23] employed CFD to enhance flow uniformity in catalytic converters, reinforcing its pertinence in the refinement of aerodynamic designs [24-28]. Research on base pressure control in high-speed flows has substantiated the efficacy of passive methodologies such as implementing quarter and semi-circular ribs. Khan *et al.,* [29] demonstrated that these ribs enhance flow reattachment and diminish base drag in suddenly expanded ducts [30-34]. Moreover, other investigations have accentuated the critical role of nozzle geometry in stabilizing flows across varying Mach numbers, revealing the vital importance of managing flow separation. Khan *et al.,* [35] presented a cost-efficient passive approach to mitigate base drag, illustrating the feasibility of aerodynamic optimization [36,37]. The effect of rib in a suddenly expanded flow at sonic Mach numbers was studied by Rathakrishnan [38]. He conducted experiments at various nozzle pressure ratios ranging from 1.141 to 2.54 for 3:1, 3:2 and 3:3 rib aspect ratios. His investigation revealed that there is a decreasing trend in the base pressure at a lower aspect ratio and control results in a decrease in the base pressure. The base pressure increased when rib with an aspect ratio of 3:3 was employed. Therefore, depending upon the end user's demands, these combinations of the ribs can be used. If the mission requirement is to increase the base pressure, then rib with an aspect ratio is ideal. The rib with an aspect ratio 3:1 is the right choice when the application is in a combustion chamber. In the present study, we have validated our CFD results first with the experimental results of Rathakrishnan [38]. After validation, we have taken various rib geometry, rib location and nozzle pressure ratios to study passive control's effect on base pressure.

Although various studies emphasize the importance of expansion geometry and cavity configurations, the synergistic effects of ribs and cavities across diverse Mach numbers warrant further investigation. Furthermore, most research is predominantly centred on static geometries; the capacity of adaptive designs to dynamically enhance flow characteristics remains substantially underexplored. This lack of inquiry is noteworthy because addressing these deficiencies could profoundly deepen our understanding of aerodynamic phenomena. As we know, the screech-prone Mach number is in the range from 1.6 to 1.8; hence, this study is conducted to assess the

effectiveness of the passive control in the form of quarter rib and the effect of rib radius and the location of rib in the duct. However, these studies show the necessity of continued research in this area, as the interdependencies among various factors remain fully understood. Although promising, this endeavour requires further investigation because the complexities involved are substantial. From the above review, there is evident research on low supersonic Mach numbers. So far, none of the researchers has ever used quarter rib circles to regulate the base flows at sonic and supersonic Mach numbers.

3. Finite Volume Method

3.1 Governing Equations

The following hypotheses are taken into consideration:

i. Turbulent flow is considered because of the turbulent viscous dissipation effects.
ii. The fluid's viscosity varies with temperature and is compressible.
iii. At atmospheric pressure, the flow exits the duct.
iv. While scanning the literature, we found that the internal flow k-epsilon turbulence model is the best as it gives reasonably good results. Sutherland's three-coefficient viscosity model is expressed as follows:

$$\mu' = \mu'_o \left(\frac{T_a}{T_{a,o}}\right)^{3/2} \frac{T_{a,o}+S\prime}{T_a+S\prime} \tag{1}$$

The reference viscosity value in kg/m-s is denoted as μ'_o,, where μ' represents the viscosity. T_a denotes static temperature; K represents the temperature of a standard reference and S' is the temperature-dependent Sutherland constant. Three-dimensional continuity equation for compressible flow:

The equation for mass balance is as follows:

$$\frac{\partial \rho}{\partial t} + \underline{\nabla} \cdot \left(\rho \underline{V}\right) = 0 \tag{2}$$

Where the fluid's velocity is denoted by V. The equation for momentum balance is:

$$\frac{\partial}{\partial t}\left(\rho \underline{V}\right) + \underline{\nabla} \cdot \left(\rho \underline{V}\underline{V}\right) + \underline{\nabla} p = \underline{\nabla} \cdot \left[2\mu\left(\underline{\nabla V}\right)_o^s\right] + \underline{\nabla} \cdot \left(\tau_{=Re}\right) \tag{3}$$

Where $\left(\underline{\nabla V}\right)_o^s = \left(\underline{\nabla V}\right)^s - \frac{1}{3}\left(\underline{\nabla} \cdot \underline{V}\right)\underline{I}$, $\left(\underline{\nabla V}\right)^s = \frac{\nabla V + \nabla V^T}{2}$ and $\tau_{=Re}$ is the turbulent stress tensor. The formulae for total energy are as follows:

$$\frac{\partial}{\partial t}\left[\rho\left(\frac{1}{2}V^2 + u_{int}\right)\right] + \underline{\nabla}\left[\rho\left(\frac{1}{2}V^2 + u_{int}\right)\underline{V}\right] = \underline{\nabla}\left(\lambda \underline{\nabla} T - p\underline{V} + 2\mu \underline{V} \cdot \left(\underline{\nabla V}\right)_o^s + \underline{V} \cdot \tau_{=Re}\right) \tag{4}$$

Where u_{int} is the internal energy and λ is the thermal conductivity. Many internal flow simulations use the k-epsilon turbulence model due to its affordability, resilience and sufficient accuracy. The Ansys Fluent program incorporates the k-epsilon (ε) turbulence model used in this research. The K-equation allowed us to calculate the turbulent kinetic energy.

$$\frac{\partial}{\partial t}(\rho k) + \underline{\nabla} \cdot (\rho \underline{V} k) = \underline{\nabla} \cdot \left[(\mu + \frac{\mu_t}{\sigma_k})(\underline{\nabla} k) \right] - \rho\varepsilon + M_x \quad (5)$$

The turbulent kinetic energy dissipation rate is denoted by ε, the turbulent Prandtl number is σ-k and the word Mx is the turbulence generation. Precisely, the dissipation (or (-equation)) is controlled by,

$$\frac{\partial(\rho\varepsilon)}{\partial t} = -\underline{\nabla} \cdot (\rho\varepsilon\vec{V}) + \underline{\nabla} \cdot \left[\left(\mu + \frac{\mu_T}{\sigma_\varepsilon} \right) \nabla\varepsilon \right] - C_1 f_1 \left(\frac{\varepsilon}{k} \right) M - C_2 f_2 \frac{\varepsilon^2}{k} \quad (6)$$

where $\mu_t = \rho f_\mu C_\mu k^2/\varepsilon$ denotes turbulent viscosity and the arbitrary constants are denoted as $\overline{C_\mu} = 0.09$, $\overline{C_1} = 1.44$, $\overline{C_2} = 1.92$, $\overline{f_\mu} = 1$, $\sigma_k = 1.0$ and $\sigma_\varepsilon = 1.3$.

3.2 Geometry and Modelling

The finite volume technique (FVM) was employed to delve further into this investigation. The CFD simulation used the ANSYS FLUENT 2024/R2 software to assess the nozzle's fluid flows. We are examining the impact of the quarter geometry of the Rib in the form of a passive control method. The orientation of the quarter rib is shown in Figure 1.

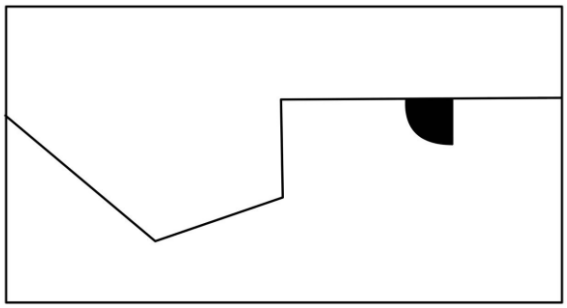

Fig. 1. Orientation of the rib

3.3 Meshing and Boundary Conditions

A crucial part of the CFD process is meshing. By choosing the free-face mesh type, the 2D model is of the structured mesh type in this case. Elements were given sizes according to each line (edge) length when the constructed structured mesh type was used. The lines were utilized to apply the element size and elements with identical forms were created using face meshing. The mesh independence check is done. Figure 2 below shows the mesh's element type and size tested during the mesh independence check.

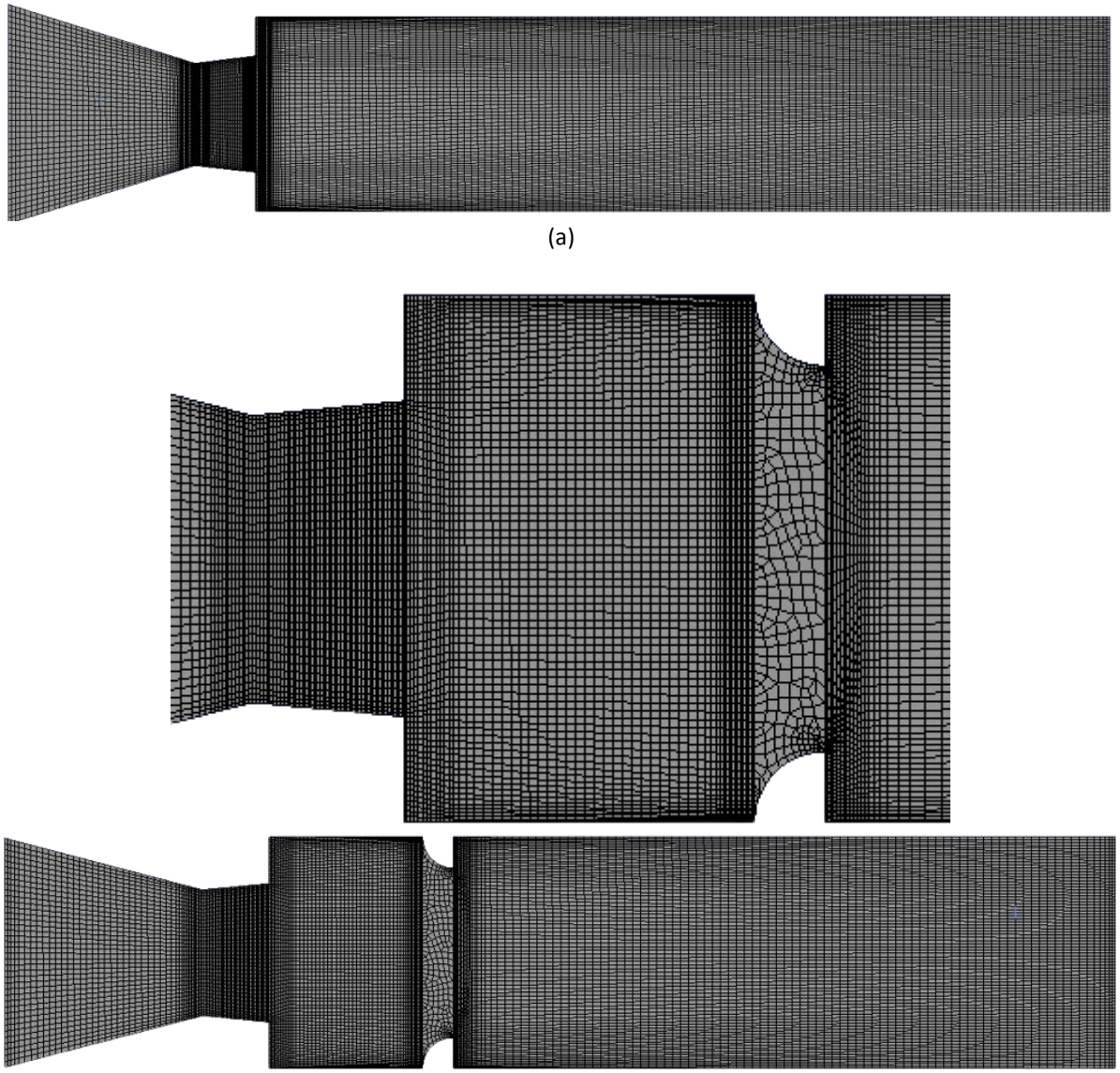

(a)

(b)

Fig. 2. Mesh model (a) Without ribs (b) With ribs

3.4 Assumptions and Fluid Properties

Assumptions are accomplished to replicate the flow activities in the precise physical environment. Appropriate mathematical and numerical models are selected to make simpler the governing equations.

To solve the governing equations simultaneously, numerical modelling requires choosing the appropriate mathematical models, such as the governing equations, boundary conditions, mesh quality and numerical method. Despite its limitations in accurately representing physical phenomena, the computational method has been trusted for decades and offers sufficient insight into flow behaviour. As a result, this calls for careful consideration of elements that closely resemble the flow behaviour. This study pinpoints the presumptions that jeopardize the precise physical state. The followings are the presumptions and characteristics covered in this study:

i. The flow is assumed to be a steady 2D flow because geometry is symmetric. Hence, the assumption that the flow is 2-D is justified.
ii. The density of the air is variable as the flow is compressible. The inlet pressure is the gauge pressure at that Mach number and NPR and at the outlet of the duct, the gauge pressure at the outlet is zero.
iii. Turbulent flow has a significant impact on turbulent viscous dissipation at a given flow velocity, so it is taken into consideration.
iv. The viscosity of the fluid is dependent on temperature.
v. At standard atmospheric pressure, the flows leave the duct. At normal ambient pressure, they do not.

Since the flow via the nozzle is considered turbulent, the compressible flow field is represented by the k-epsilon standard model. The subsequent equations most appropriately characterize the turbulent flow.

3.5 Geometry of the Model

The ANSYS Workbench program utilized fluid flow (Fluent) analytical techniques throughout the computational fluid dynamics (CFD) procedure. The model was generated via a Design Modeler. Figure 3 depicts a converging nozzle that abruptly widens into a duct with five ribs. Rathakrishnan [38] experimental setup, the dimensions of the convergent-divergent nozzle with a suddenly expanded duct are as stated below.

Table 1
The geometries of the validation model

Parameters	Dimensions
Nozzle inlet diameter	30 mm
Nozzle outlet diameter	10 mm
Duct diameter	22 mm
Duct length	Varies from 1D to 6D
Converging length	20 mm
Rib width	3 mm
Rib height	Varies from 1mm to 3mm

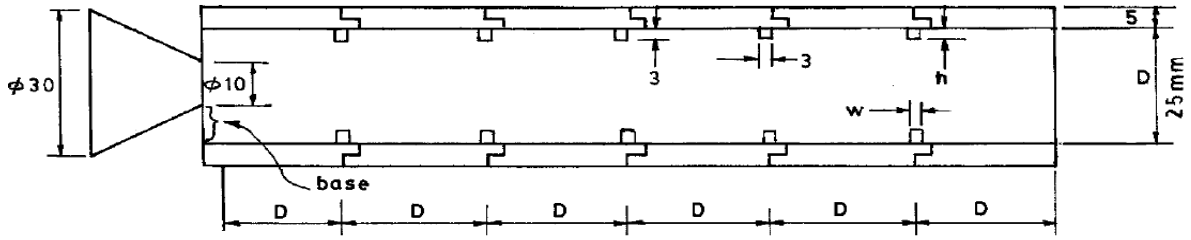

Fig. 3. Duct with five ribs used in an experimental study [38]

3.6 Validation of Previous Work

According to Rathakrishnan [38], the prior work was performed at aspect ratios of 3:3, 3:2 and 3:1; an area ratio of 6.25; L/D ranging from 1 to 6; pressure ratios of 1.141, 1.295, 1.550, 1.707 and 2.458; and nozzle exit Mach numbers of 0.44, 0.62, 0.82, 0.91 and 1.0. However, in a prior publication by Rathakrishnan [38], the result from Figure 4 with NPR (P01/Pa) 2.458 and models with control in

the form of ribs with aspect ratios 3:2 and 3:3 was chosen to be compared to the current work. The simulation is supported by Rathakrishnan [38] experimental work, which used five ribs positioned at equidistant intervals in the duct, as illustrated in Figure 4. The results of base pressure fluctuation with NPR of 2.458 and L/D ranging from 2 to 6 are obtained. The study is repeated to validate the numerical results of a model with control over different rib aspect ratios [38].

.

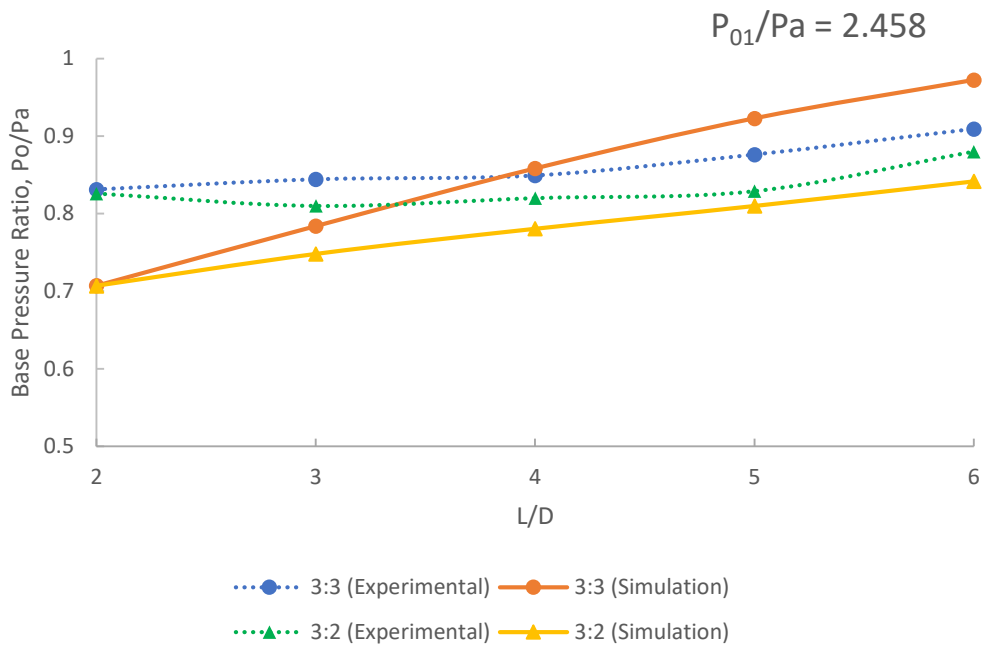

Fig. 4. Validation of previous work by Rathakrishnan [38]

Figure 4 demonstrates the current and earlier studies' base pressure ratio data curves [38]. The experimental values were denoted by dotted lines, while the simulation results obtained using ANSYS Fluent were represented by straight lines. The present numerical analysis exhibited a percentage discrepancy of less than 10% compared to the previous experimental study. Consequently, the current work met the criteria for acceptability. The curves exhibited a consistent pattern, with each point close to the subsequent one. As a result, based on the table and graph described before, the validation of the current work was successful.

3.7 Mesh Independence Study

Table 2 provides data from a mesh independence study, a crucial step in computational simulations to ensure that the results remain consistent regardless of the mesh refinement level. The element sizes range from the course to the finest, with corresponding node and element counts for each mesh configuration. As the mesh becomes finer, the number of nodes and elements increases significantly, from 1,284 nodes and 1,145 elements in the coarsest mesh to 1,354,262 nodes and 1,351,303 elements in the finest mesh.

This study aims to determine the optimal mesh size for accurate simulations without unnecessary computational expense. The table shows a notable increase in nodes and elements as the mesh is refined. The coarsest mesh has relatively few nodes and elements, which means lower computational cost but potentially less accuracy. Conversely, the finest mesh offers the highest resolution at the

expense of significant computational resources. The medium and fine meshes provide intermediate levels of refinement, offering a balance between accuracy and efficiency.

Table 2
Mesh independence study

Element size	Coarsest	Coarse	Medium 1	Medium 2	Fine	Finer	Finest
Nodes	2997	3534	9582	17216	101106	293204	1482632
Elements	2808	3320	9720	16818	100248	291720	1479348

Based on the trends in node and element numbers, the finest mesh will likely produce the most accurate results (Figure 5). However, continuing to refine the mesh beyond a certain point may offer diminishing returns in terms of accuracy while significantly increasing computational time. A critical assessment of this table would suggest that the "Fine" or "Finer" mesh configurations may represent the best balance between accuracy and computational efficiency. These configurations substantially increase nodes and elements compared to the medium meshes without reaching the computational expense of the finest mesh. If simulation results do not significantly change between the fine and finest meshes, further refinement to the finest mesh is unnecessary, as it would only increase the computational time without added benefit. Thus, the fine or finer mesh sizes are likely the best choices for further simulation.

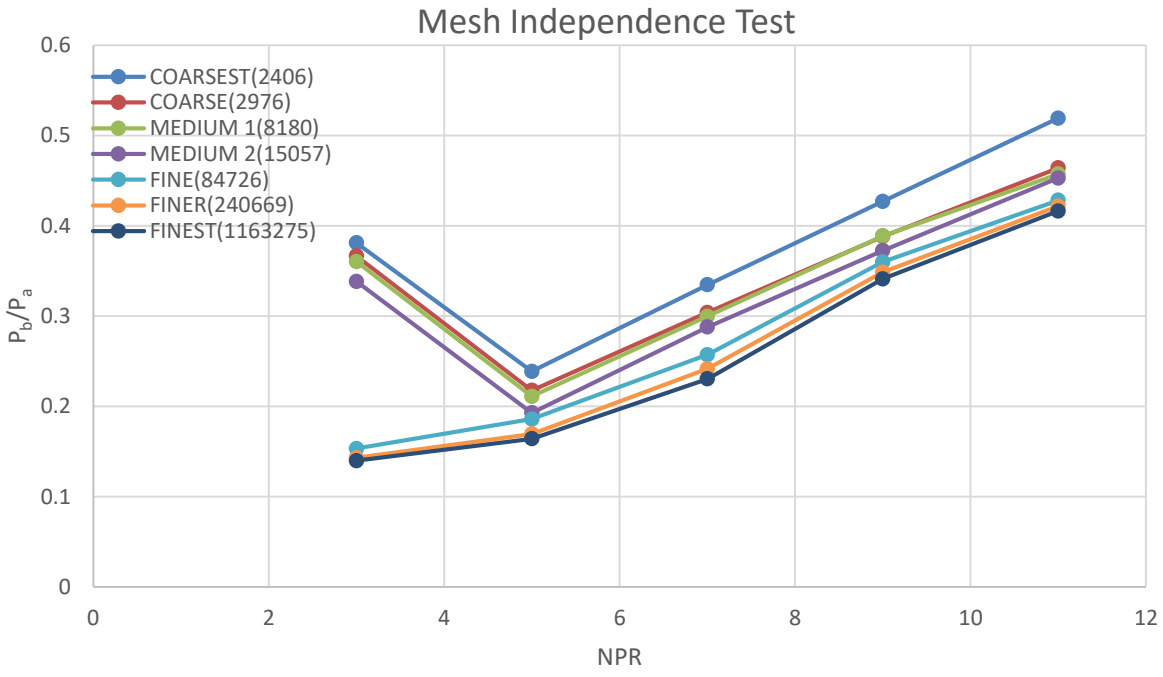

Fig. 5. Results of mesh check

4. Results and Discussion

It would be interesting to comprehend the mechanics driving the suddenly expanded flow field before evaluating the data. The nozzle exit boundary layer would develop as a free shear layer and meet the enlarged duct wall downstream. The location of the flow attachment is known as the reattachment point. The distance from the base to the termination of the reattachment is known as the reattachment length. There will be one or more vortices between the reattachment point, the

base and the free shear layer edge. The primary vortex pumps fluid from the base to the main flow on the other side of the free shear layer edge and is the first and most vital closest to the base. Low pressure at the base is the outcome of this pumping action. But because vortex shedding is periodic, the pumping likewise becomes periodic. That leads to fluctuations in the base pressure.

On the other hand, the base pressure variations were negligible and could be stated as a mean value. Due to the vortex motion's periodicity, the duct's whole flow field oscillates. The oscillations might become severe when specific geometrical parameters and flow are combined.

The primary vortex strength is controlled by the flow Mach number and the reattachment and it also has a significant effect on the flow oscillations in the duct and the amount of suction at the base. For supersonic Mach values, the nozzle outlet has either an expansion fan ring, Mach waves or an oblique shock ring, depending on whether the flow is under, correct or over-expanded. When there is an expansion, the flow quickens and veers off; combining this additional twisting and the turning resulting from the free expansion will cause early reattachment and shorter reattachment length. The flow will be directed towards the duct centreline in the event of an oblique shock, which will cause the reattachment process to be prolonged and delayed. As a result, since the primary vortex drives base pressure and flow field oscillations, waves will always substantially affect strength. The flow will meet more vortices shed at the hollow if the duct features annular ribs. These smaller vortices may operate as mixing promoters, raising the base pressure.

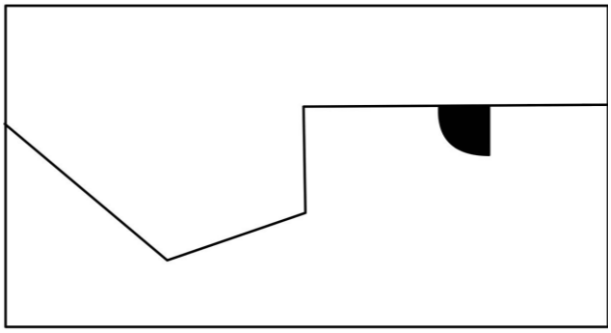

Fig. 6. A view of the nozzle, duct and rib assembly

4.1 Base Pressure Results for Rib Location 0.5D

For a duct diameter of 22 mm, various rib radii ranging from 1 mm to 4 mm and duct lengths from L = 1D to 6D, this study was carried out at Mach M = 1.8. In this study, the NPRs vary from 3 to 11. The expansion levels for the NPRs under study are 0.52, 0.87, 1.22, 1.57 and 1.91 and the NPR required for proper expansion is 5.75. The NPR range utilized in this test causes the jet to over-, correct and under-expand as it leaves the nozzle. For both over- and under-expanded conditions, it is well-known that an oblique shock or expansion fan will be positioned at the nozzle lip. One may understand how the degree of expansion impacts the base pressure with and without control by looking at the base pressure variation as a function of Mach number, L/D and NPR.

Along with L/D, the NPRs include data on base pressure for over-, correctly and under-expanded jets. If there's an oblique shock at the nozzle exit, the shock will bend the shear layer from the nozzle toward the nozzle centre line for an over-expanded case. That will make the reattachment take longer than in a scenario without a shock. As is well known, changes in the reattachment length affect the base pressure and vortex.

Similarly, an expansion fan shortens the reattachment length by directing the shear layer that exits the nozzle in the direction of the base as opposed to a case without one when the nozzle is

under-expanded. Due to their ability to produce an oblique shock or expansion fan at the nozzle exit, over- and under-expansion operations are essential to base pressure analysis. According to the results, the base pressure level is influenced by variables besides over- and under-expansion. However, the degree of under- or overexpansion determines the base pressure level.

When the quarter-circle rib is positioned at 11 mm from the base, with varying rib radii ranging from 1 mm to 4 mm, for varied duct lengths ranging from L = 22 mm to L = 132 mm at different levels of expansion, the results of this study are displayed in Figure 7(a) to Figure 7(f). The results of this investigation are shown in Figure 7(a) for the most petite duct lengths of 22 mm. This duct length yields different base pressure results than the other lengths. This pattern is caused by the duct's shortest length, which makes it impossible for the flow to adhere to the duct wall. In addition, the ambient pressure will be strongly influenced, potentially affecting the duct's internal flow field.

For a rib radius of 1 mm and in the absence of a rib, the base pressure shows a downward trend with and without control till the nozzle reaches NPR = 7. The base pressure does, however, tend to increase when NPR is seven and above, except for rib radii of 3 and 4 mm, because these ribs are positioned to produce robust vortices and drive more mass into the base area, raising the base pressure. At NPR 11, the base pressure ratio values are 0.5, 0.75, 1.2, 1.5 and 2.0, in that order. Depending on the application, the users may take a final call about the rib radius, duct length and nozzle pressure ratio (NPR). If the mission requirement is to enhance the base pressure by 50%, then a 1 mm rib radius is ideal.

The magnitude of the base pressure data is almost the same for all duct lengths, except for slight differences that are to be expected given the duct size variances. Their values will fluctuate due to variations in the duct size and ambient pressure's varying influence.

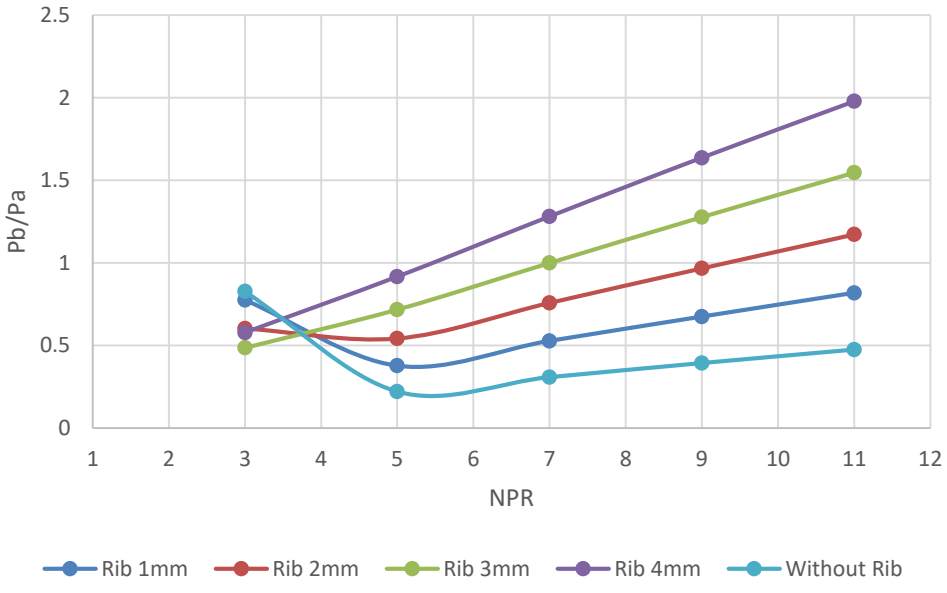

(a) L/D = 1

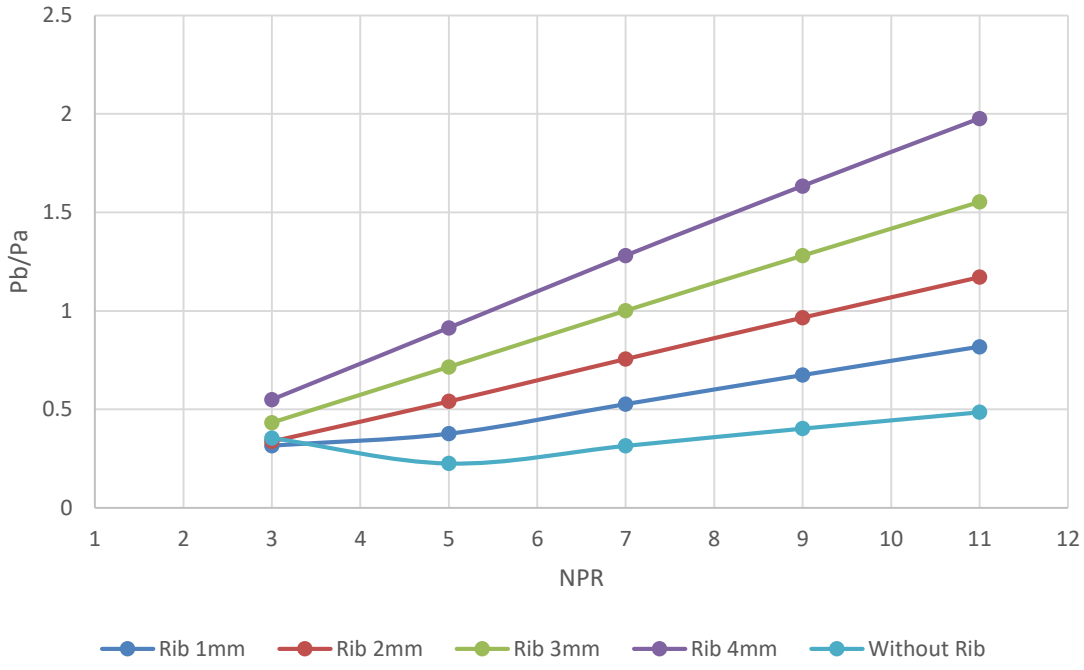
2.5
2
1.5
1
0.5
0
Pb/Pa
1
2
3
4
5
6
7
8
9
10
11
12
NPR
Rib 1mm
Rib 2mm
Rib 3mm
Rib 4mm
Without Rib

(b) L/D = 2

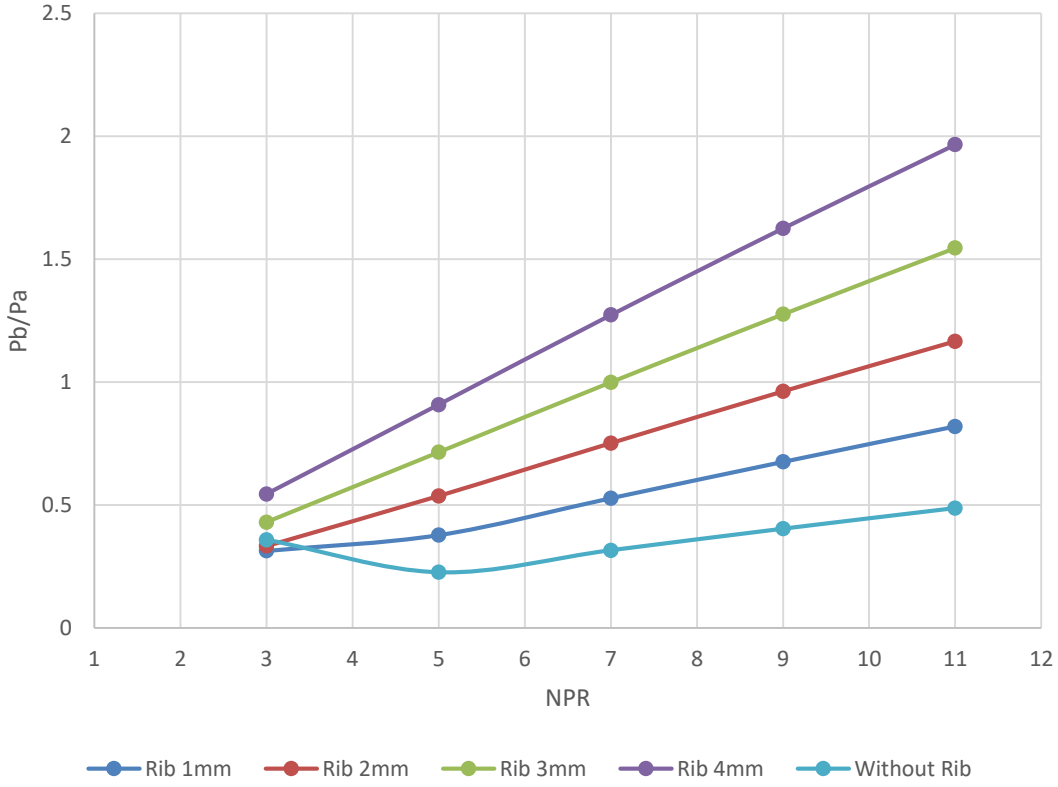
2.5
2
1.5
1
0.5
0
Pb/Pa
1
2
3
4
5
6
7
8
9
10
11
12
NPR
Rib 1mm
Rib 2mm
Rib 3mm
Rib 4mm
Without Rib

(c) L/D = 3

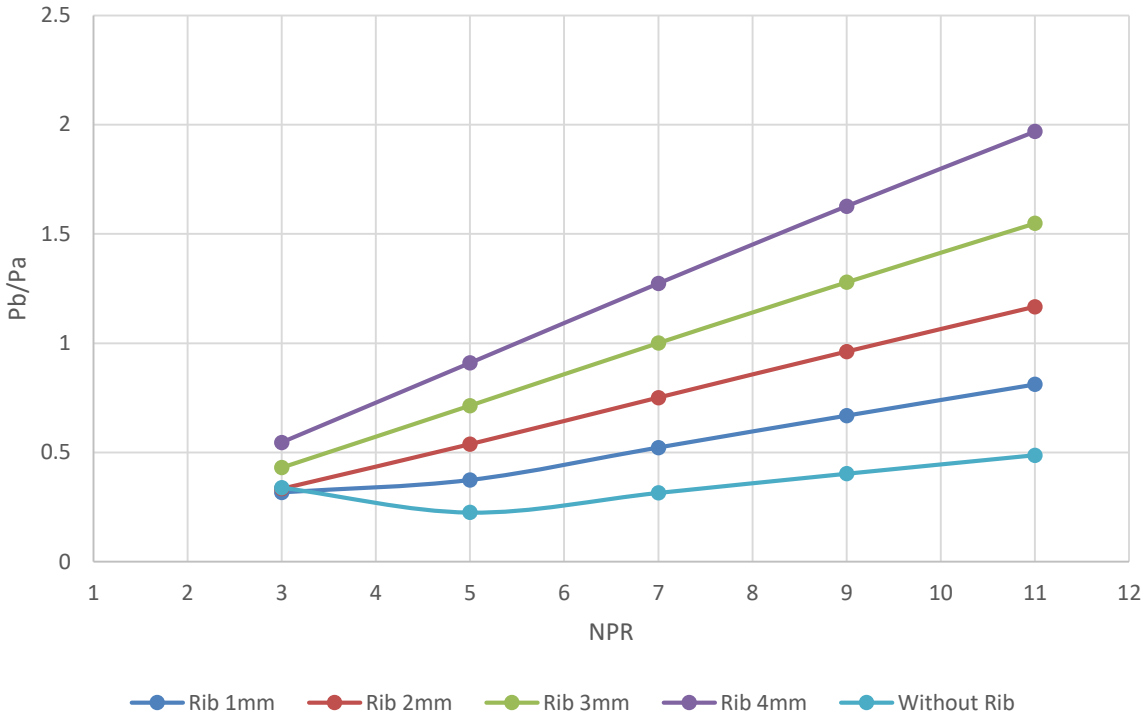
2.5
2
1.5
1
0.5
0
Pb/Pa
1
2
3
4
5
6
7
8
9
10
11
12
NPR
Rib 1mm
Rib 2mm
Rib 3mm
Rib 4mm
Without Rib

(d) L/D = 4

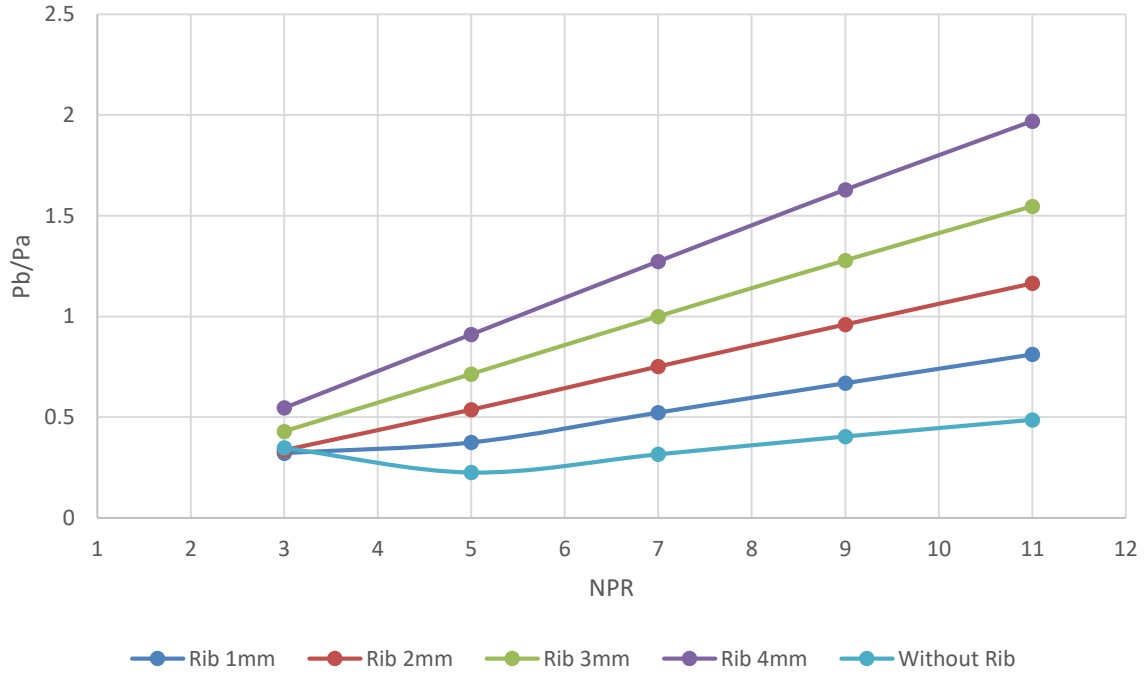
2.5
2
1.5
1
0.5
0
Pb/Pa
1
2
3
4
5
6
7
8
9
10
11
12
NPR
Rib 1mm
Rib 2mm
Rib 3mm
Rib 4mm
Without Rib

(e) L/D = 5

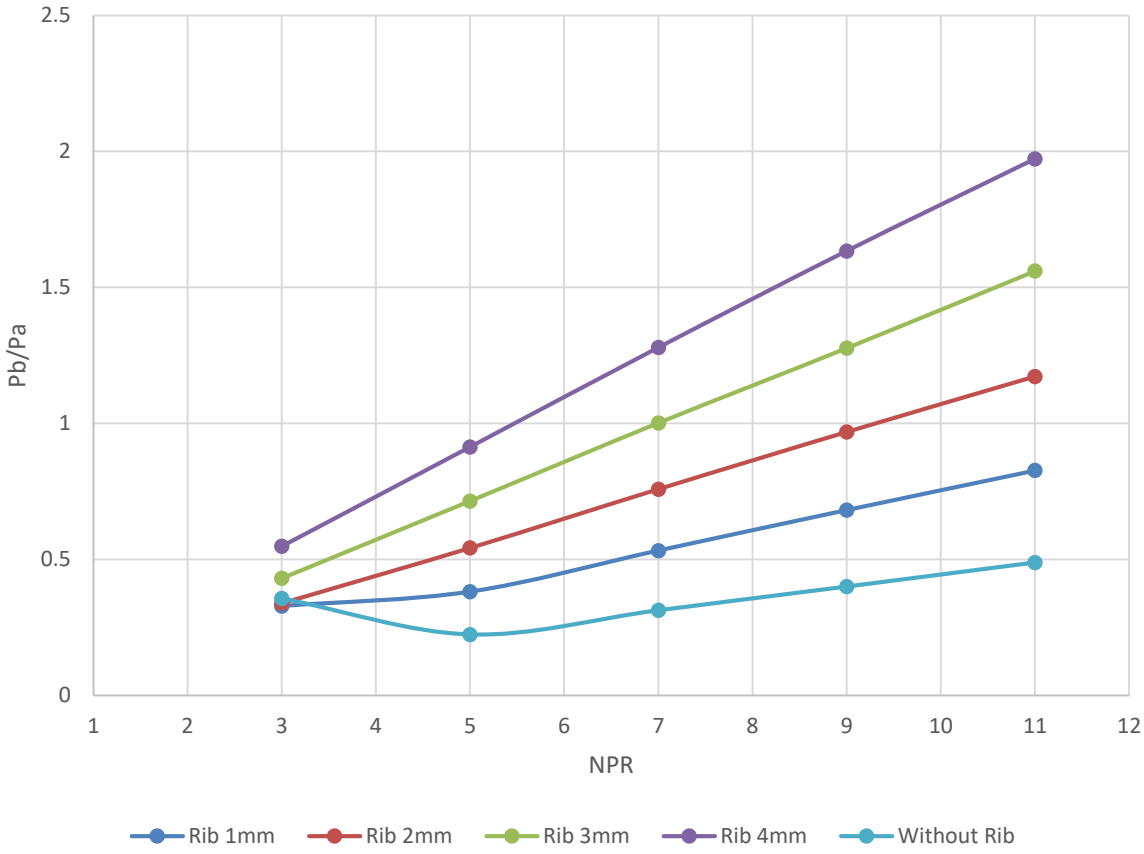

(f) L/D = 6

Fig. 7. Base pressure vs. NPR for various duct lengths

4.2 Base Pressure Results for Rib Location 1D

Figure 8(a) to Figure 8(e) show the findings of this study when the rib is placed 22 mm from the base where the rib radii range from 1 mm to 4 mm, having duct sizes in the range 1D to 6D at various expansion levels ranging from NPRs 3 to 11. These results have distinct differences, especially for the rib 11 mm from the base. A rib of radius 1 mm, which was very effective and could reduce the suction and increase the base pressure by 60%, has become ineffective. The base pressure values without control and with control for a 1 mm rib radius are the same as the passive control in the form of a 1 mm rib, which cannot influence the flow field inside the duct. However, when we look at the effect of the rib with a 2mm radius, it is found that the control has become marginally more efficient, resulting in a marginal rise in the base pressure values. Similarly, we look at the base pressure results for the remaining ribs having radii of 3 mm and 4 mm and the base pressure values attained are nearly the same as was seen for rib location 11 mm Figure 8(a).

Similar results are seen in Figure 8 (b) to Figure 8(e) for duct lengths 2D to 6D, for the same rib radius ranges and for the same NPRs ranging from 3 to 11. Since only duct lengths change, negligible and unnoticeable variations are observed for these duct sizes.

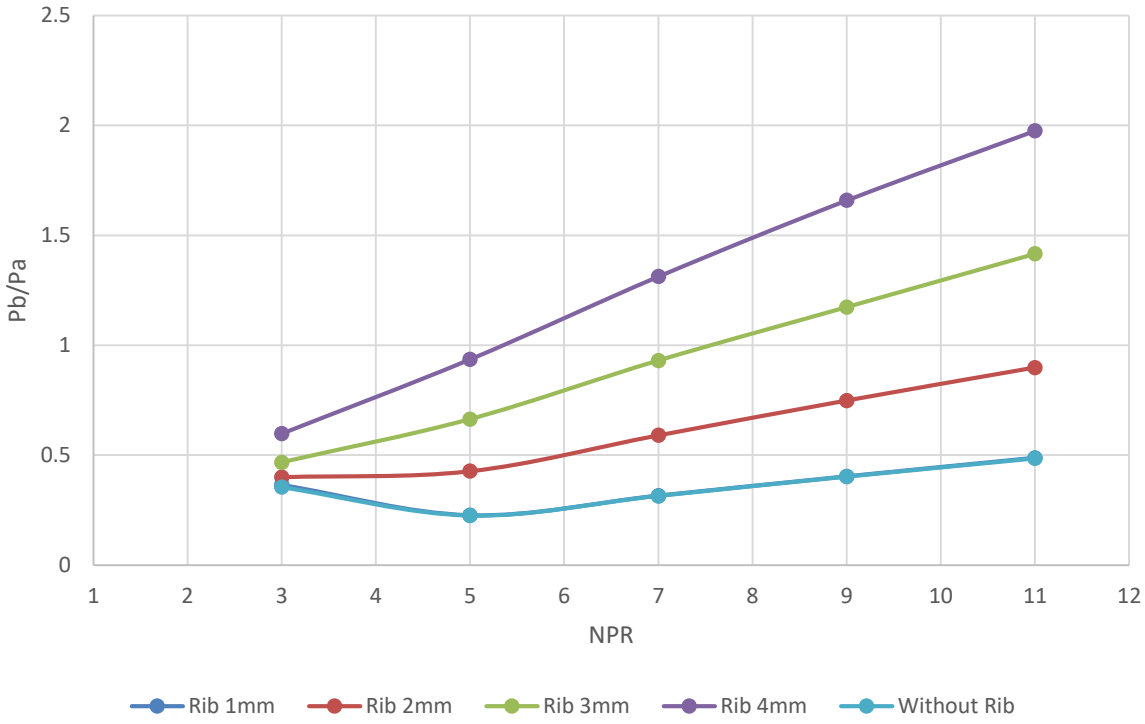
2.5
2
1.5
1
0.5
0
Pb/Pa
1
2
3
4
5
6
7
8
9
10
11
12
NPR
Rib 1mm
Rib 2mm
Rib 3mm
Rib 4mm
Without Rib

(a) L/D = 2

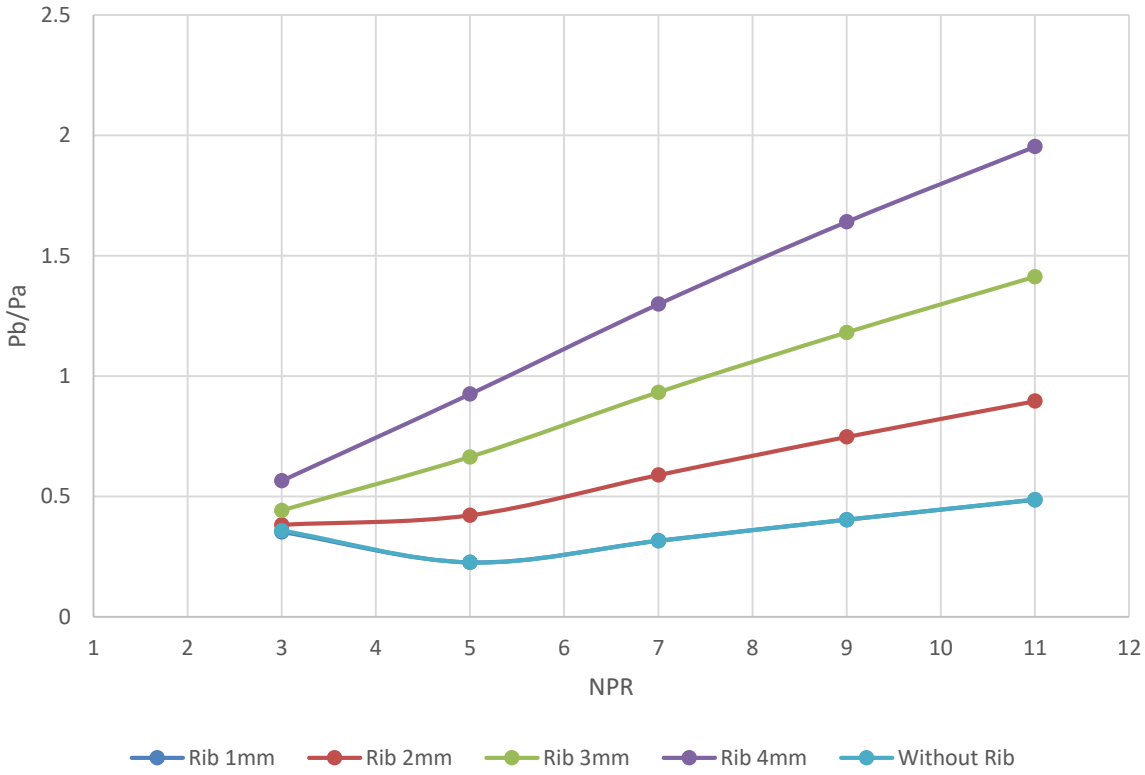
2.5
2
1.5
1
0.5
0
Pb/Pa
1
2
3
4
5
6
7
8
9
10
11
12
NPR
Rib 1mm
Rib 2mm
Rib 3mm
Rib 4mm
Without Rib

(b) L/D = 3

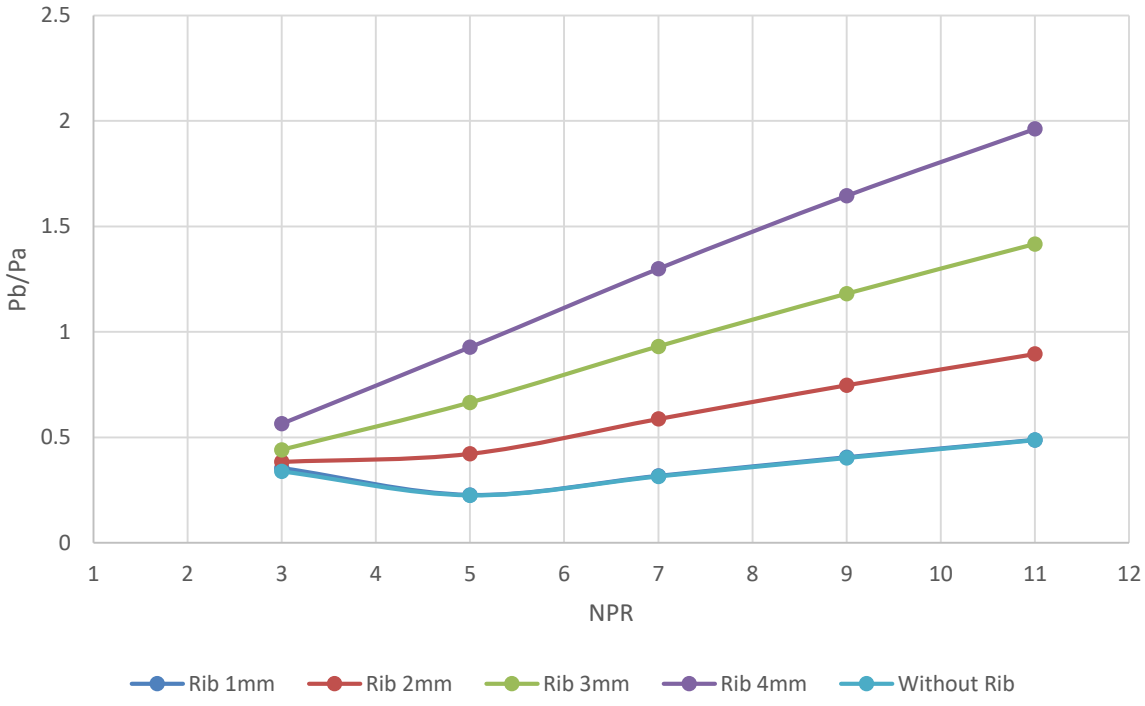
2.5
2
1.5
1
0.5
0
Pb/Pa
1
2
3
4
5
6
7
8
9
10
11
12
NPR
Rib 1mm
Rib 2mm
Rib 3mm
Rib 4mm
Without Rib

(c) L/D = 4

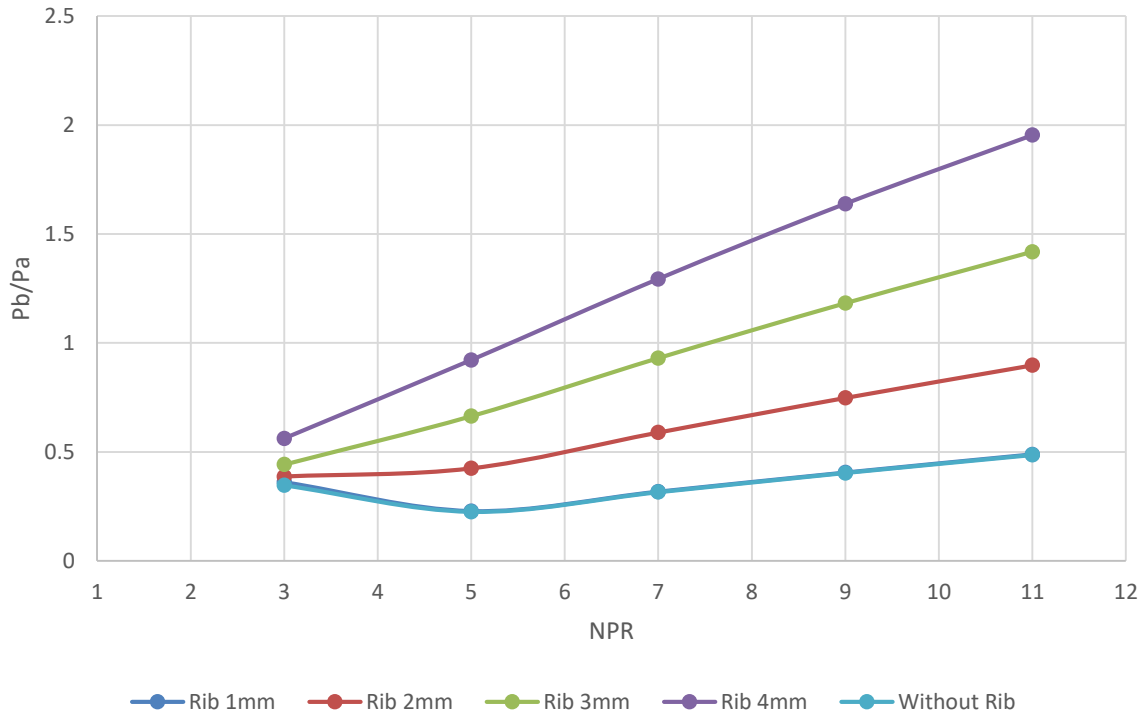
2.5
2
1.5
1
0.5
0
Pb/Pa
1
2
3
4
5
6
7
8
9
10
11
12
NPR
Rib 1mm
Rib 2mm
Rib 3mm
Rib 4mm
Without Rib

(d) L/D = 5

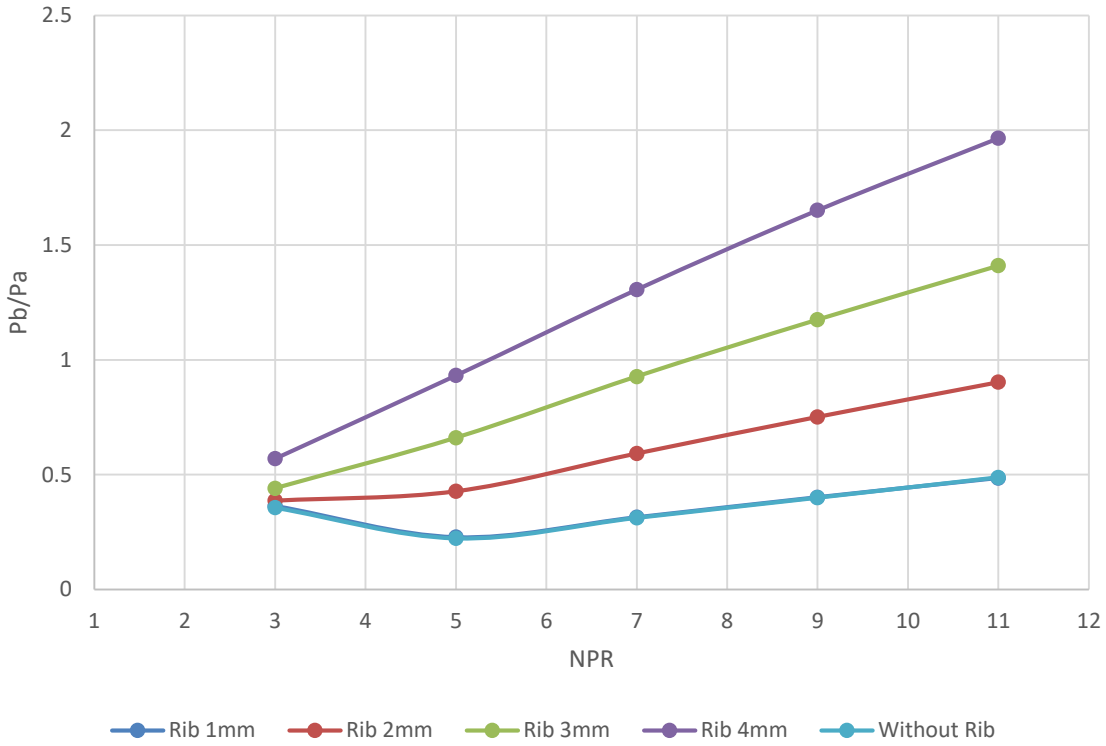

(e) L/D = 6

Fig. 8. Base pressure vs. NPR for various duct lengths

4.3 Base Pressure Results for Rib Location 1.5D

When ribs are located at 33 mm from the base, the base pressure results for different radii from 1 mm to 4 mm, for the same range of the duct lengths and NPRs are shown in Figure 9(a) to Figure (e). As the rib has further moved downstream 11 mm more distance from the previous rib location, there is an overall increase in the base pressure ratios and their values are 1.1, 1.8 and 2.6 for rib radii 2 mm, 3 mm and 4 mm, respectively. This change in the base pressure may be attributed to the rib's location, the dividing streamline's interaction and the secondary vortex created by the rib's sharp corner, as seen in Figure 9(a). With further increases in the duct sizes to 3D, 4D, 5D and 6D, the base pressure ratios are nearly the same, with marginal changes in magnitude. These changes in the base pressure ratios are due to the influence of the ambient atmospheric pressure, which will dominate for lower duct sizes. In the case of the more considerable duct length, the impact of the length will be minimized.

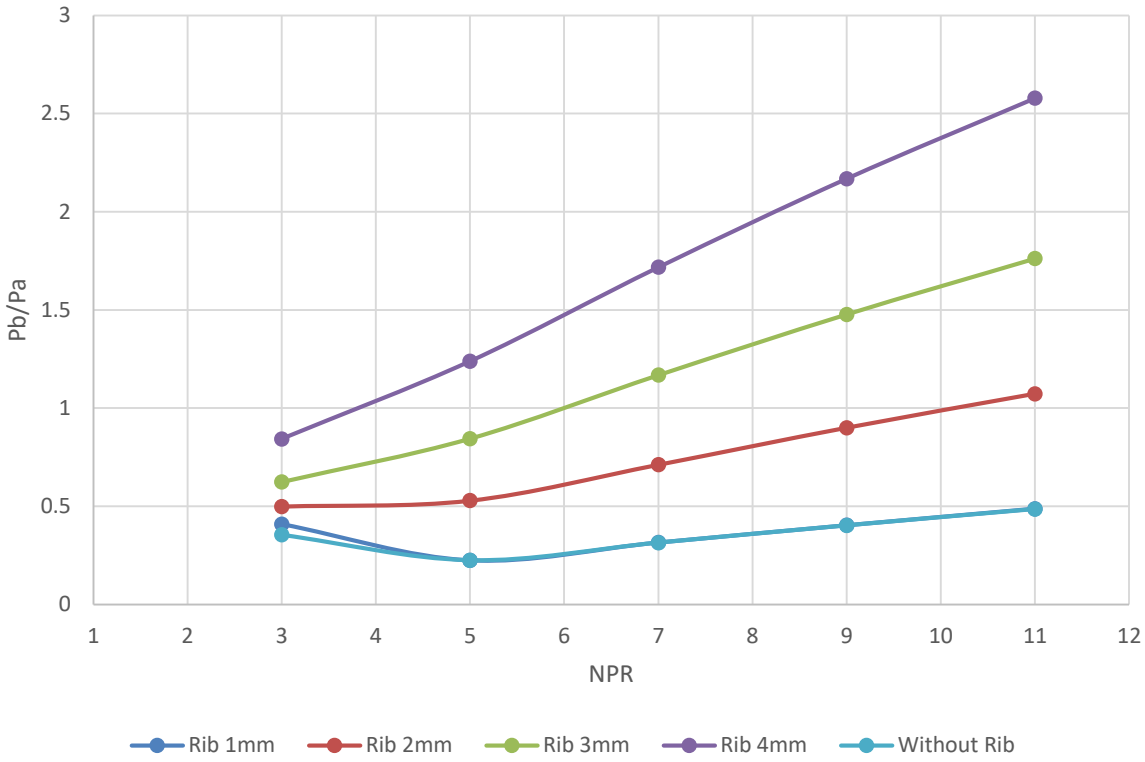
Pb/Pa
NPR
Rib 1mm
Rib 2mm
Rib 3mm
Rib 4mm
Without Rib

(a) L/D = 2

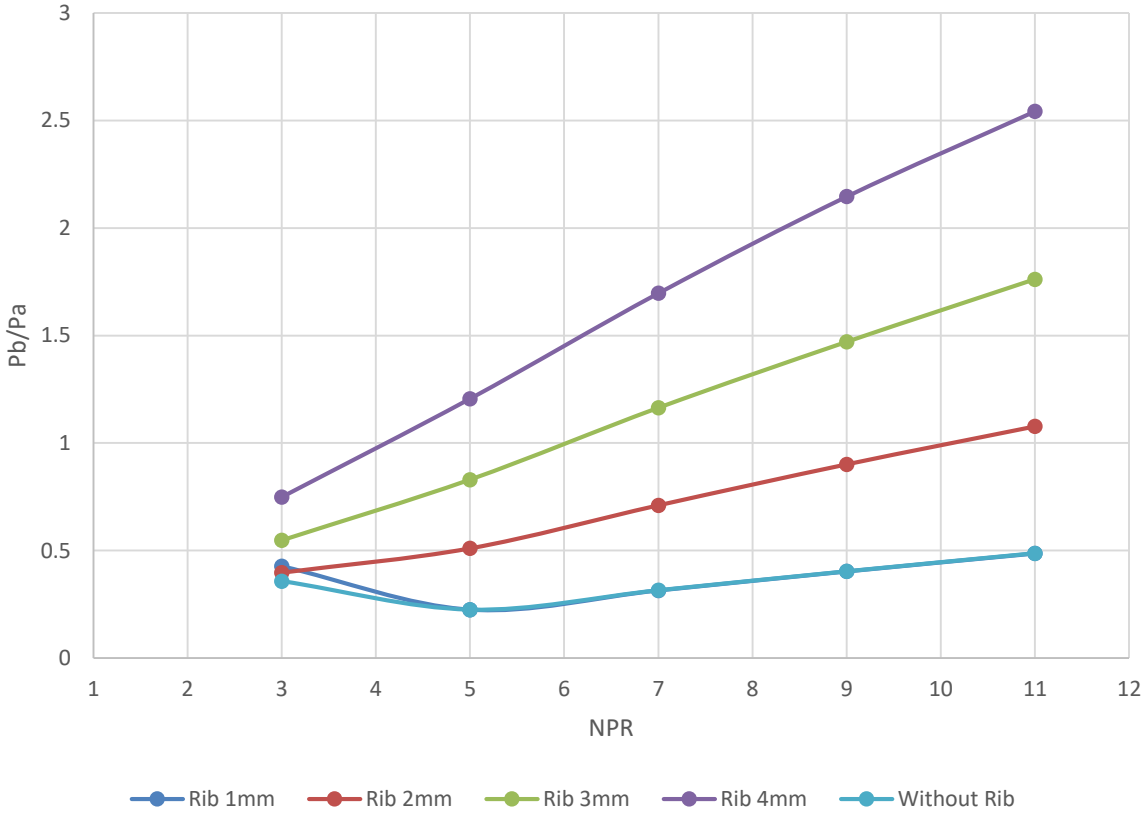
Pb/Pa
NPR
Rib 1mm
Rib 2mm
Rib 3mm
Rib 4mm
Without Rib

(b) L/D = 3

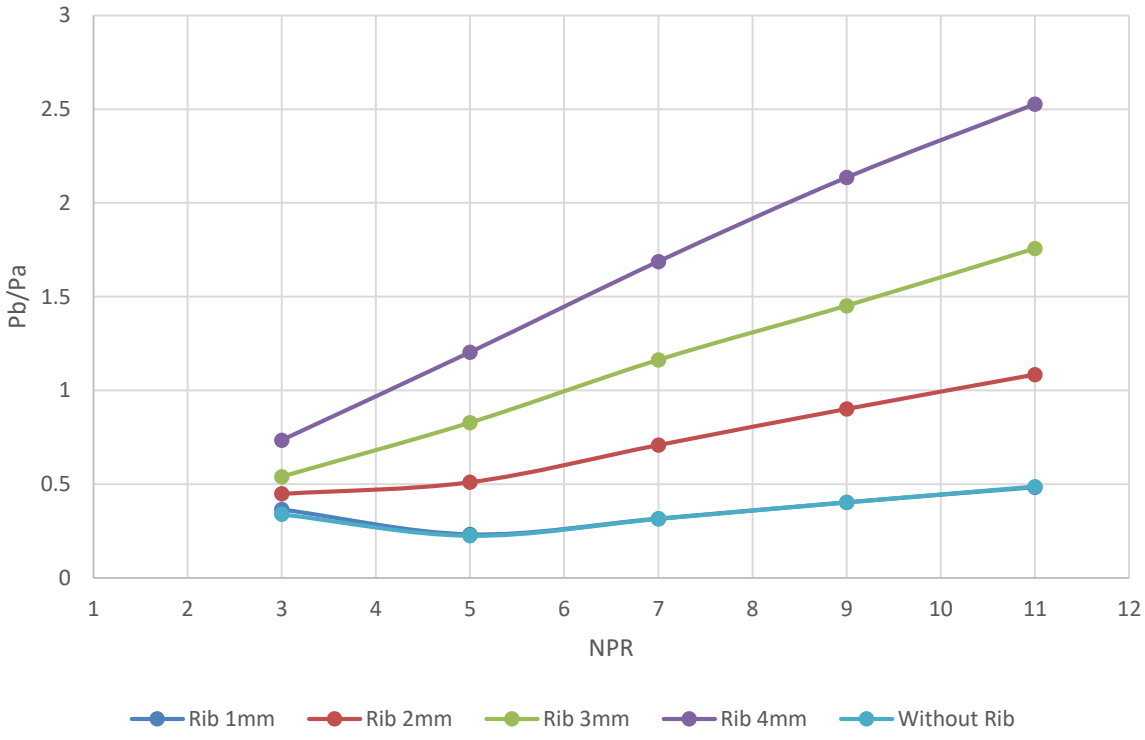
Pb/Pa
NPR
Rib 1mm
Rib 2mm
Rib 3mm
Rib 4mm
Without Rib

(c) L/D = 4

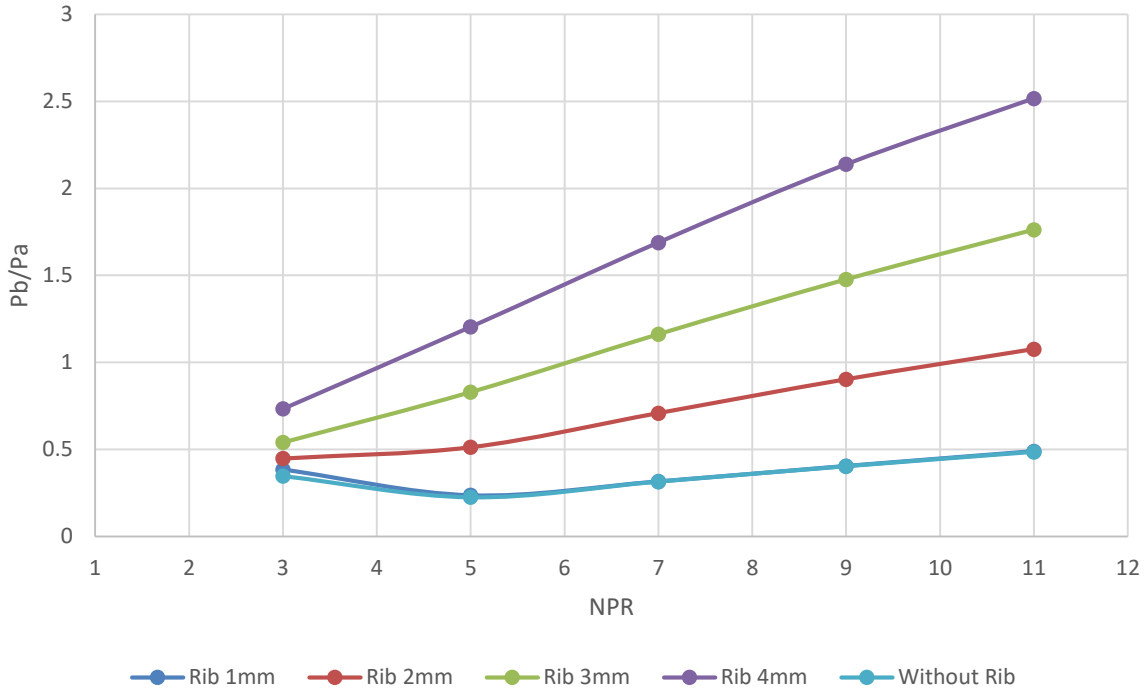
Pb/Pa
NPR
Rib 1mm
Rib 2mm
Rib 3mm
Rib 4mm
Without Rib

(d) L/D = 5

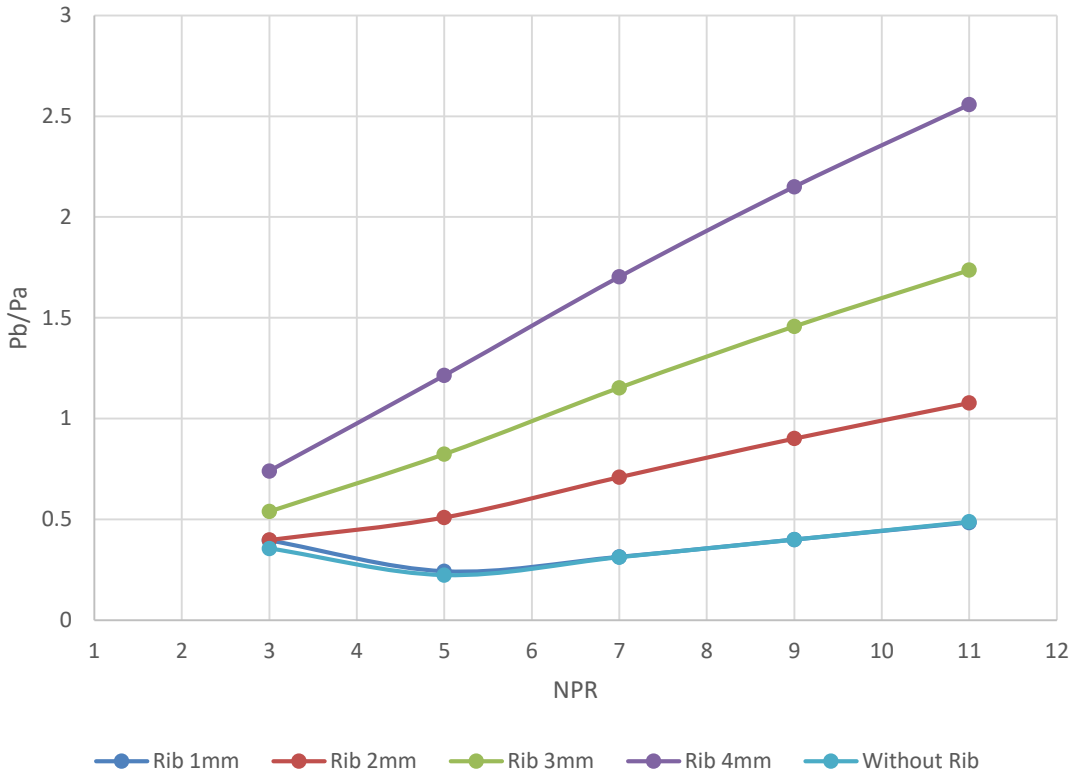

(e) L/D = 6

Fig. 9. Base pressure vs. NPR for various duct lengths

4.4 Base Pressure Results for Rib Location 2D

For the rib location of 44 mm from the base, the outcomes of this simulation study are shown in Figure 10(a) to Figure 10(d) for four radii of the ribs ranging from 1 mm to 4 mm, duct sizes from 66 mm to 132 mm for expansion levels 0.52 to 1.91. As seen earlier, the base pressure values for 1 mm rib radius and without control remained equal except during NPRs ranging from 3 to 5. This pattern in the base pressure may be due to the presence of the oblique shock waves at the nozzle exit; however, the strength of the shock waves gets reduced and the nozzles which were flowing under the influence of adverse pressure gradient will be facing ideally expanded conditions and with further increase in the nozzle pressure ratio nozzle will undergo through an expansion fan due to the favourable pressure gradient. It is well known that passive or active control mechanisms become effective once nozzles flow under the influence of the favourable pressure gradient.

From Figure 10(a) for duct length 66 mm, the findings of the study indicate that passive control in the form of the quarter rib is effective and base suction is wholly eliminated for rib radii 2 mm, 3 mm, 4 mm and resulting base pressure ratios are 1.25, 2 and 3. Furthermore, it is seen that due to the shift of control mechanisms in the form of ribs, there is a further rise in the base pressure values when further shifted downstream. The reasons for this increase in the base pressure may be attributable to the fact that the rib placement seems to be very close to the reattachment point. Due to this closeness of the control mechanism, it will interfere with the secondary vortices generated by the rib; there will be an interaction between the shock waves/ Mach waves/ expansion waves and also the interaction between the dividing streamline and the boundary layer which push additional mass towards the recirculation region of the base increasing the base pressure.

Similar outcomes of the present study are seen for more considerable duct lengths, namely L = 88 mm, 110 mm and 132 mm, respectively. The base pressure values for these three duct lengths are

nearly the same except for a slight variation due to the ambient atmospheric pressure's decreased impact on the duct's flow field.

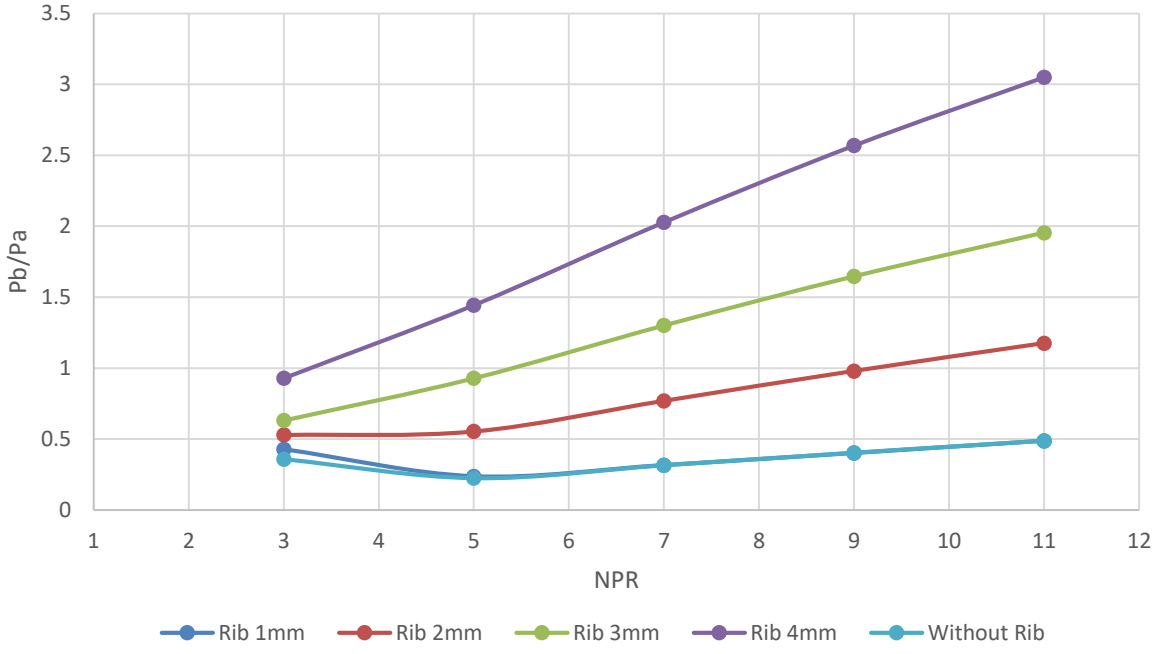

(a) L/D = 3

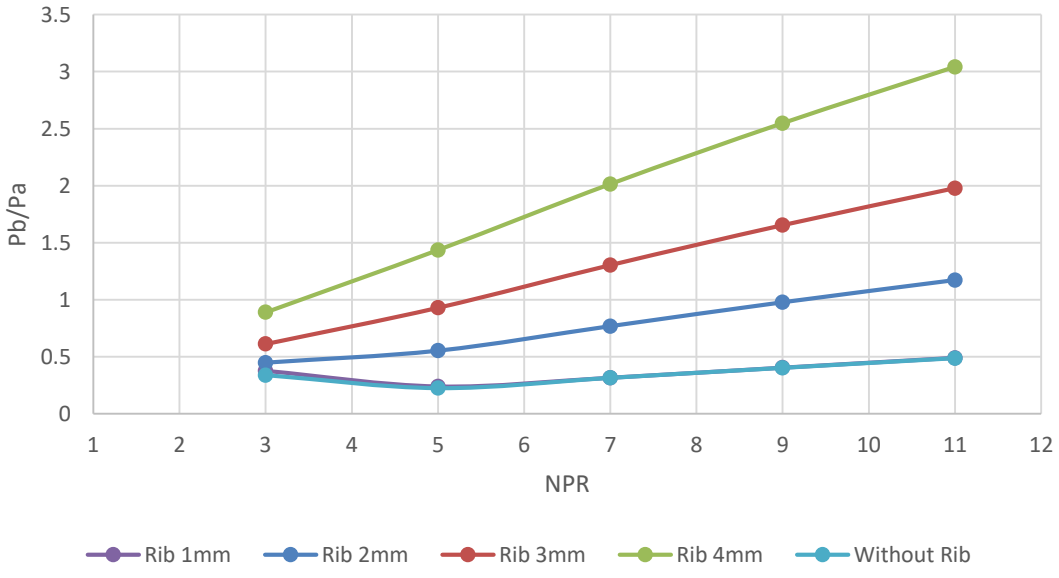

(b) L/D = 4

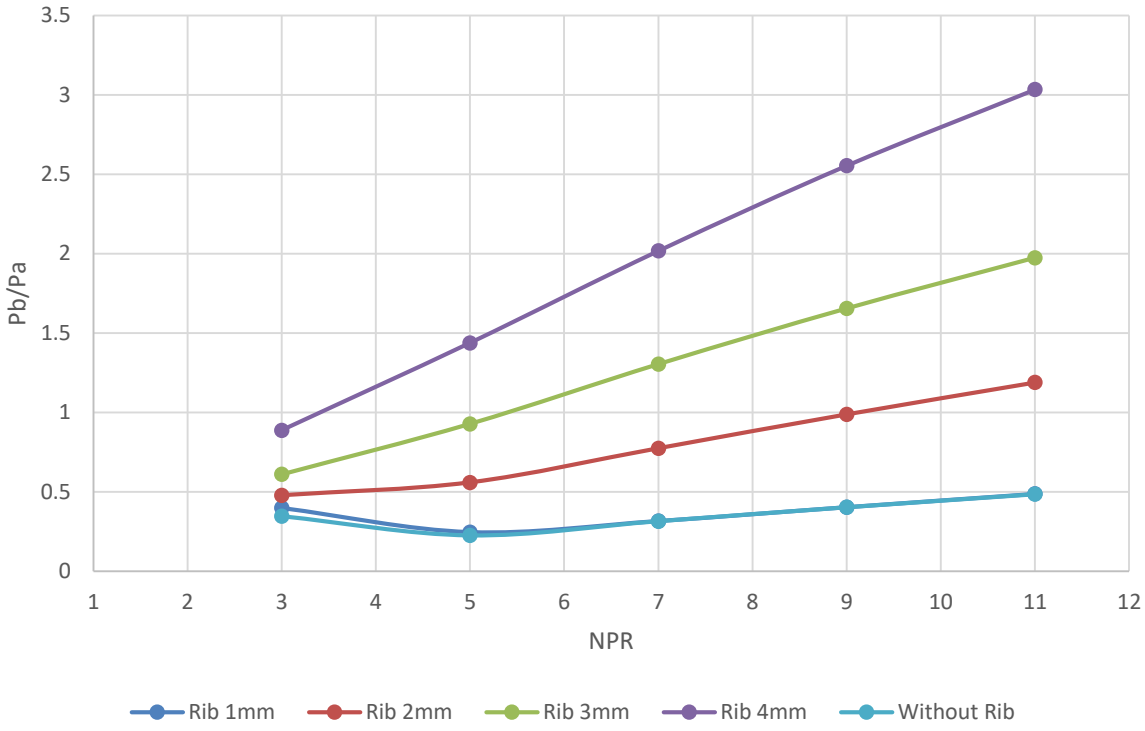

(c) L/D = 5

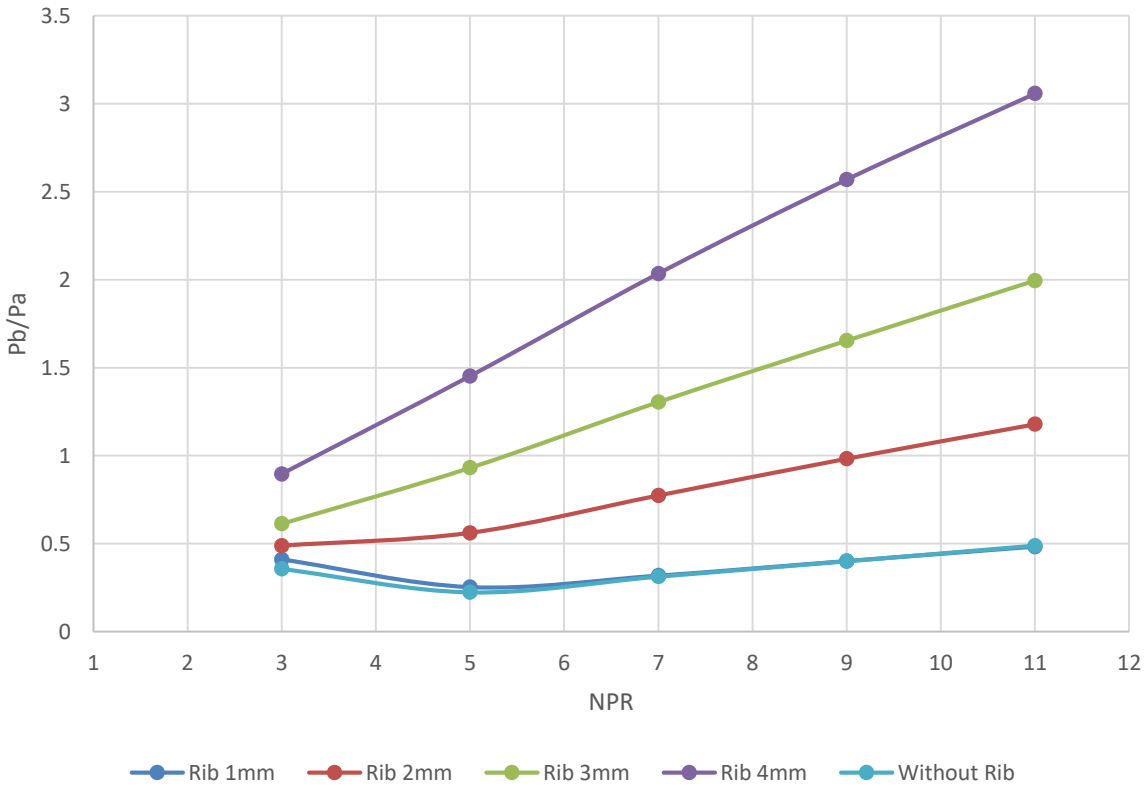

(d) L/D = 6

Fig. 10. Base pressure vs. NPR for various duct lengths

4.5 Base Pressure Results for Rib Location 3D

Figure 11(a) to Figure 11(c) present the findings of this numerical analysis for rib location of 66 mm located at the base of the duct, for various radii ranging from 1 mm to 4 mm, for duct lengths from 66 mm to 132 mm for levels of expansion in the range from 3 to 11. Base pressure results for this rib location differ from those of the rest of the rib locations. A 1 mm rib was ineffective for all the rib locations and the base pressure values for those without control and with control having a 1 mm rib radius were identical. This peculiar pattern of the base pressure is seen when the rib is placed at 3D locations, possibly because of the location of the reattachment point, which is also expected to be at 3D. Under these circumstances, when the vortex generated at the 3D location of the rib and dividing streamline will have an excessive exchange of momentum, there will be an increase in the base pressure. Hence, even though the rib radius is 1 mm, it can eliminate the suction created by the base vortex and the base pressure is equal to the ambient pressure. Therefore, a rib with a 1 mm radius is still helpful if the mission requirement is to eliminate the suction created by the base vortex and attain base pressure equal to ambient atmospheric pressure. If the user requires to achieve base pressure many folds of the ambient atmospheric pressure, then depending on the need, one can use 2 mm, 3 mm and 4 mm rib radii, respectively.

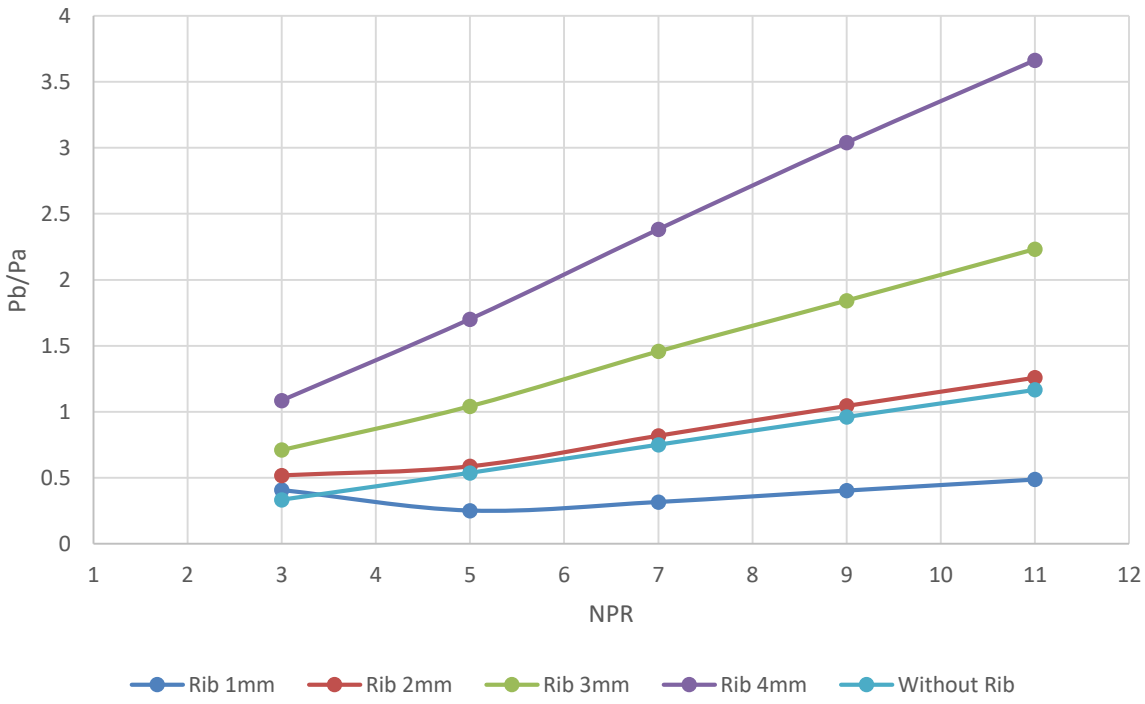

(a) L/D = 4

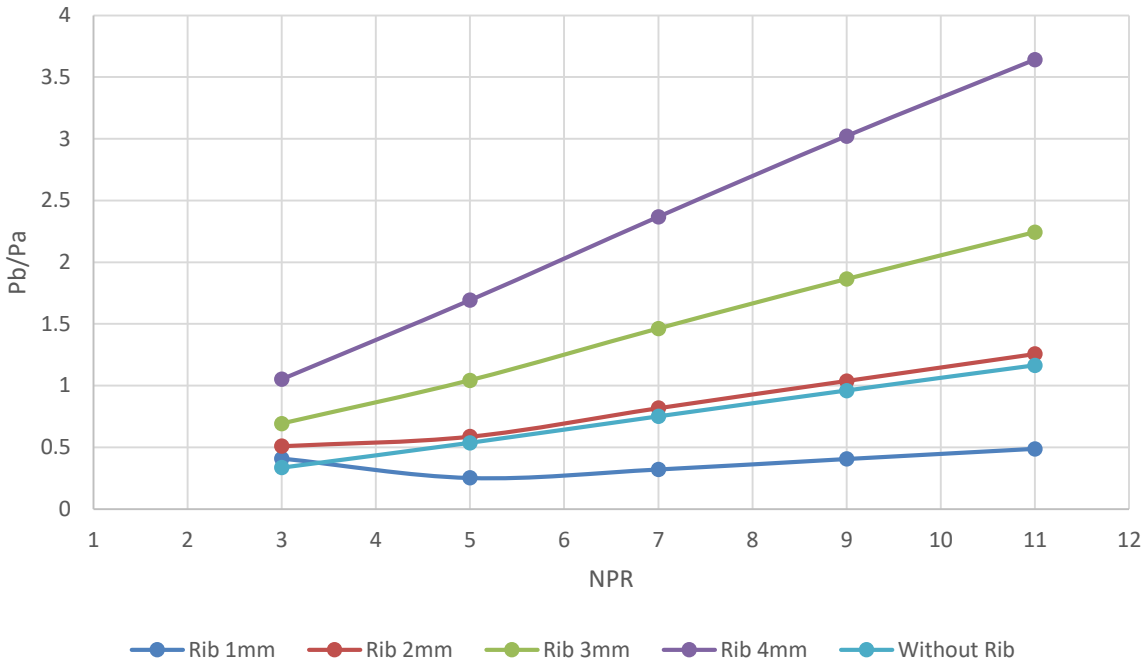

(b) L/D = 5

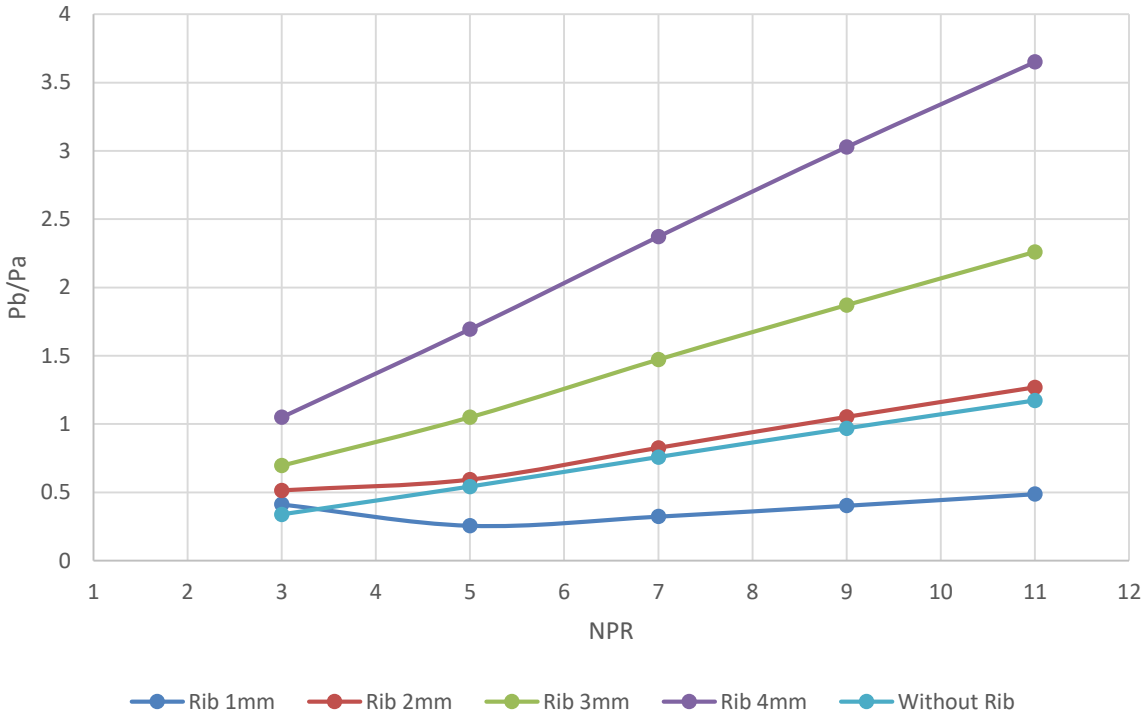

(c) L/D = 6

Fig. 11. Base pressure vs. NPR for various duct lengths

4.6 Pressure Contours for Rib Diameter 4 mm, NPR=11, L/D Ratio=6 and Various Rib Locations

Figure 12(a) to Figure 12(e) define pressure contours corresponding to a rib diameter of 4 mm, a Nozzle Pressure Ratio (NPR) of 11 and a duct length-to-diameter ratio (L/D) of 6. The findings are exhibited for various rib positions throughout the duct: 0.5D, 1D, 1.5D, 2D and 3D. However, the

implications of these variations merit further analysis because they could influence the overall fluid dynamics significantly.

The base pressure remains relatively low when the rib is located at 0.5D. The persistence of flow separation and recirculation zones is noteworthy. This phenomenon suggests that, although various control mechanisms may be employed, their efficacy remains constrained. However, it is essential to consider the underlying fluid dynamics because they significantly influence the behaviour of flow patterns in this context.

When rib is located at 1D, a slight improvement in base pressure is observed. However, the rib commences to diminish suction within the separated flow region. This observation aligns with the abstract's finding that ribs positioned closer together begin to exhibit effectiveness. Although minor changes, they emphasize rib placement's significance in aerodynamic contexts.

A more pronounced base pressure enhancement is evident when the rib is at 1.5D. The rib at this location exhibits superior control; this contributes to both flow reattachment and a diminished recirculation zone. Such observations are consistent with elevated base pressure values at intermediate rib positions. However, it is essential to recognize that these improvements occur because of the intricate dynamics at play. Although the results are promising, further analysis is warranted to understand the underlying mechanisms fully.

Further improvement is evident when the rib is located at 2D: the base pressure has increased significantly. That suggests a form of effective passive control; however, one must consider the various factors that may influence these outcomes. Although the results are promising, further investigation is necessary to fully understand the implications of these changes because they could have broader applications in the field.

The highest base pressure values are observed when the rib is at 3D. The placement of ribs at increased intervals (for instance, 66 mm or 3D) results in the most pronounced enhancement of base pressure in the duct and decreases the base drag. This phenomenon occurs even when considering smaller rib radii; however, the relationship remains noteworthy. Although one might assume that rib size could mitigate these effects, the data suggests otherwise.

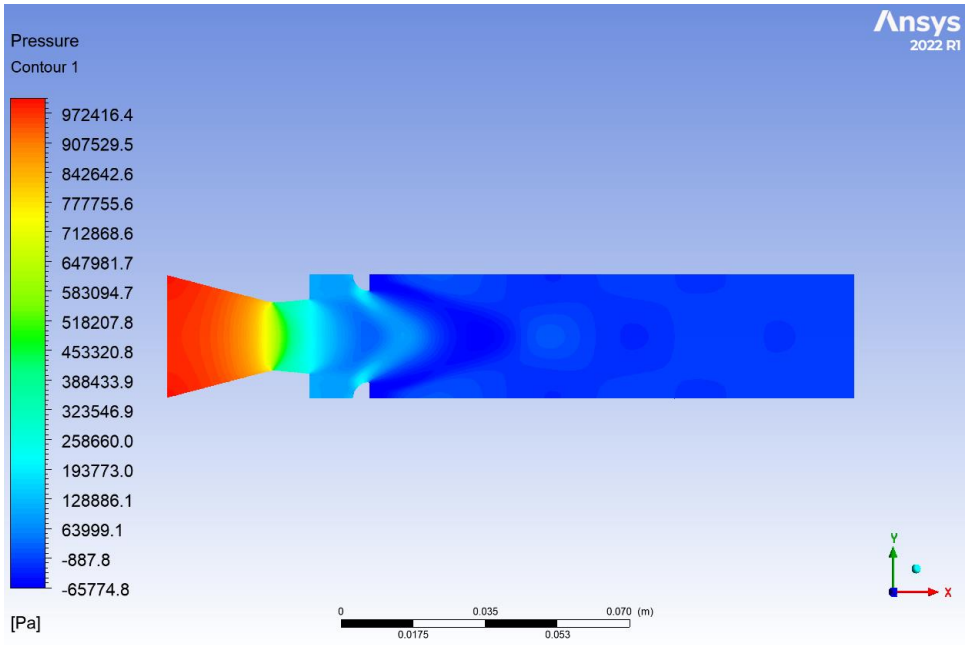

(a) Rib location 0.5D

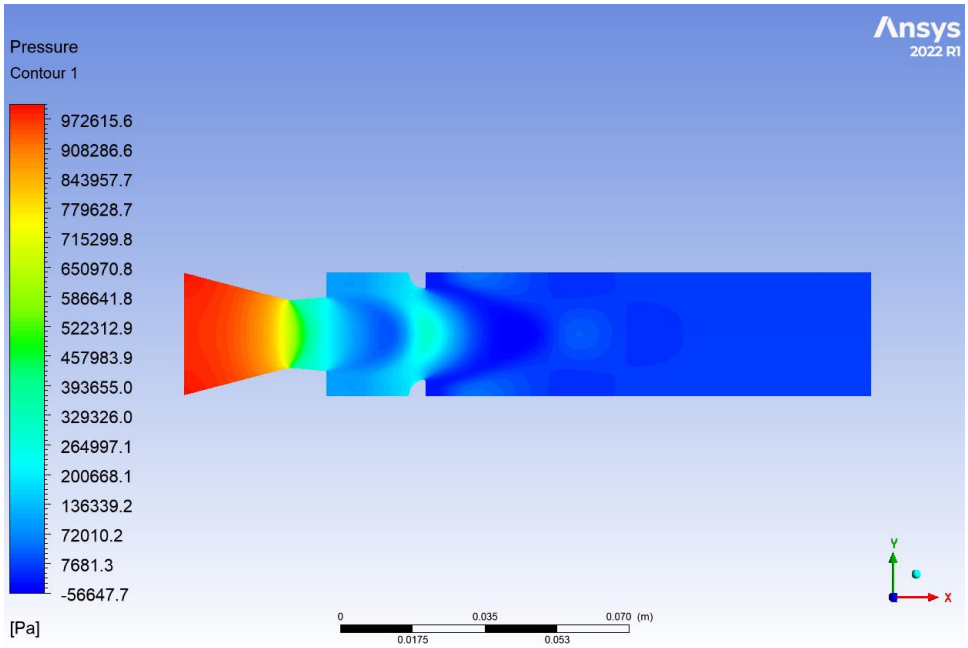

(b) Rib location 1D

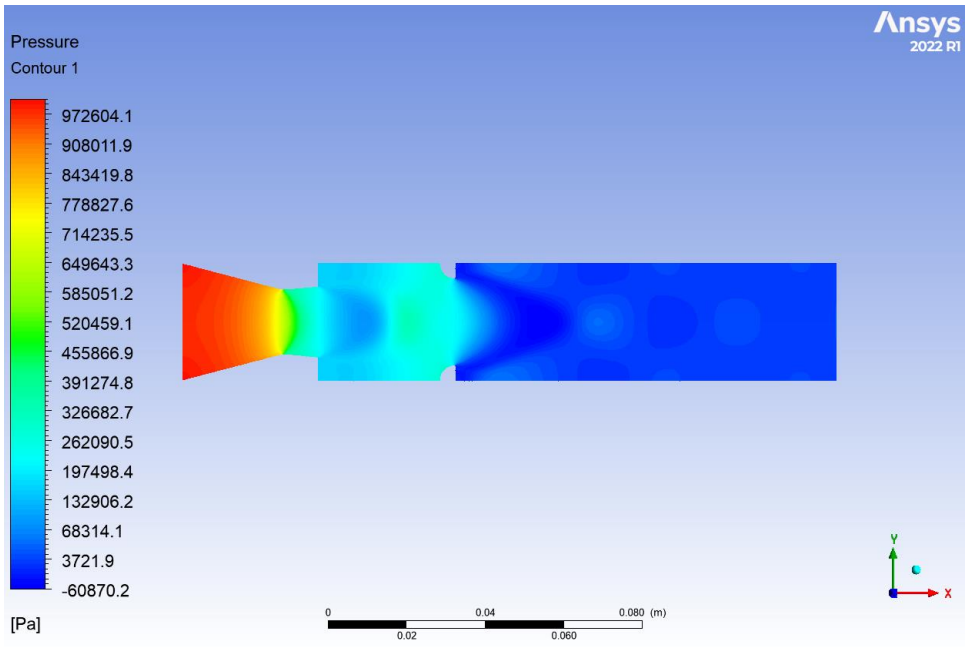

(c) Rib location 1.5D

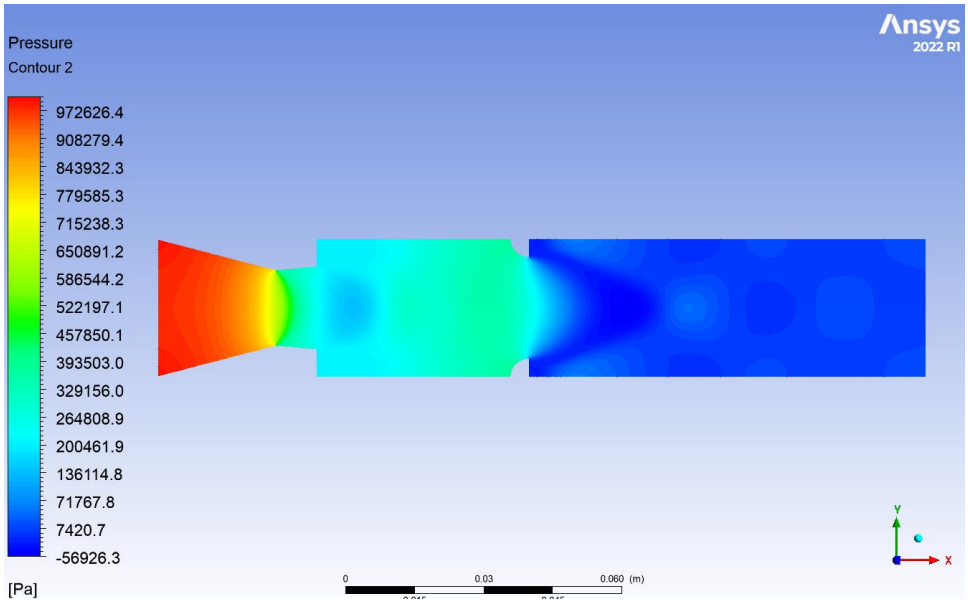

(d) Rib location 2D

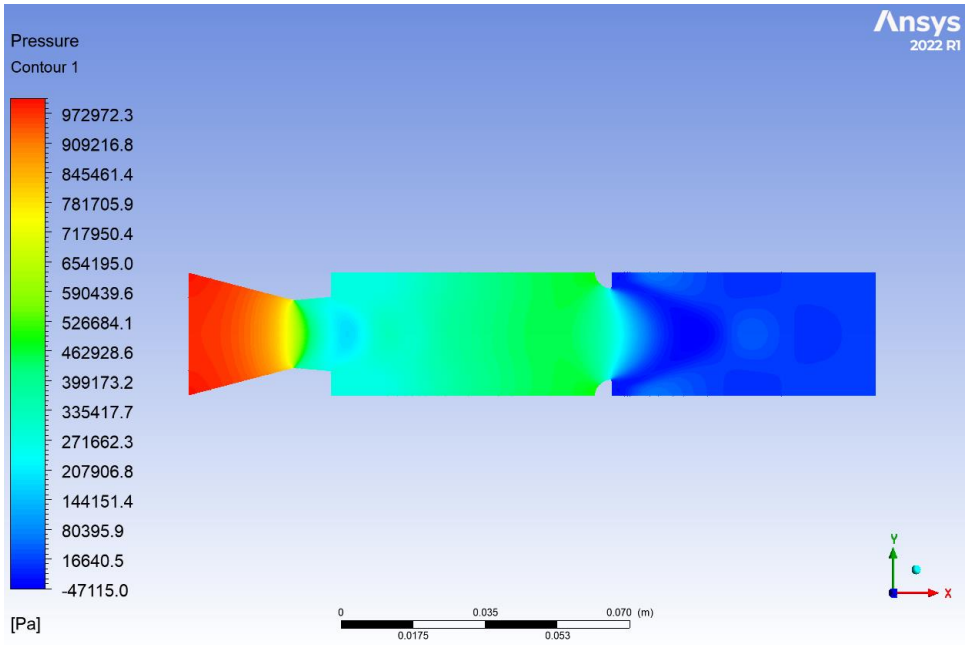

(e) Rib Location 3D

Fig. 12. Pressure contours for rib diameter 4 mm, NPR =11, L/D ratio = 6 and various rib locations

4.7 Velocity Contours for Rib Diameter 4 mm, NPR = 11, L/D Ratio = 6 and Various Rib Locations

Figure 13(a) to Figure 13(e) clarify the velocity distribution within the duct, specifically for a rib diameter of 4 mm, a Nozzle Pressure Ratio (NPR) of 11 and an L/D ratio of 6. Different rib locations along the duct are depicted: 0.5D, 1D, 1.5D, 2D and 3D.

When the rib is located at 0.5D, regions of high velocity are predominantly concentrated near the centre; however, substantial recirculation zones exist at the base. When the rib is located at 1D, a slight reduction in the size of the recirculation zone occurs, accompanied by an increase in flow velocity near the wall. When the rib is located at 1.5D, more distinct reattachment patterns and diminished low-velocity zones emerge. When the rib is located at 2D, enhanced flow reattachment

and diminished recirculation result in a more uniform velocity distribution. When the rib is located at 3D, the most pronounced reattachment occurs alongside minimal recirculation zones and high-velocity regions adjacent to the walls.

The velocity contours substantiate the study's conclusions: Downstream rib placements (2D and 3D) exhibit the most efficacious flow stabilization and reattachment. Near-nozzle placements (such as 0.5D), however, provide limited control.

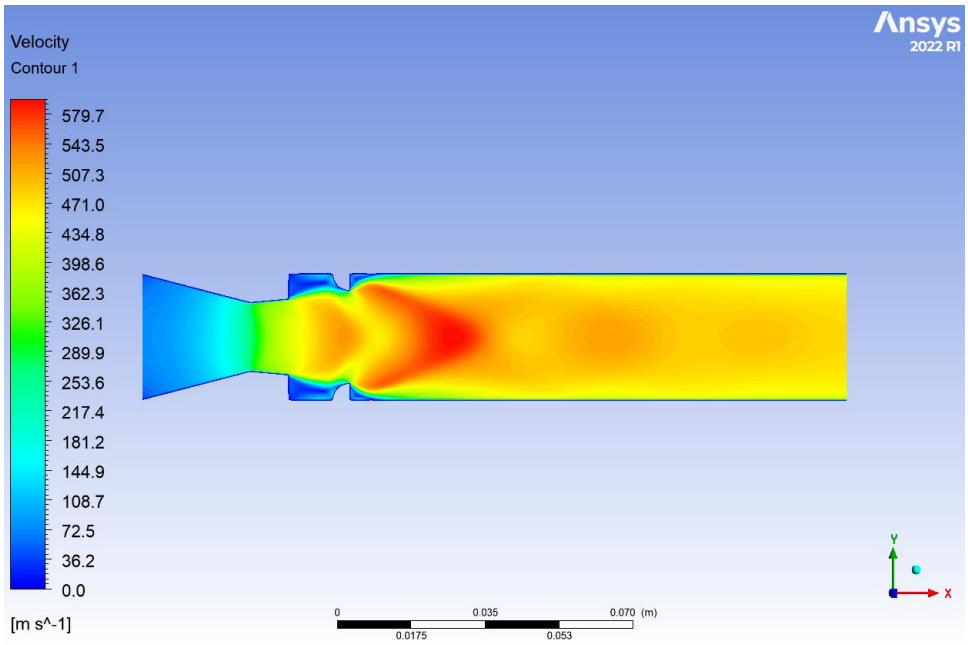

(a) Rib location 0.5D

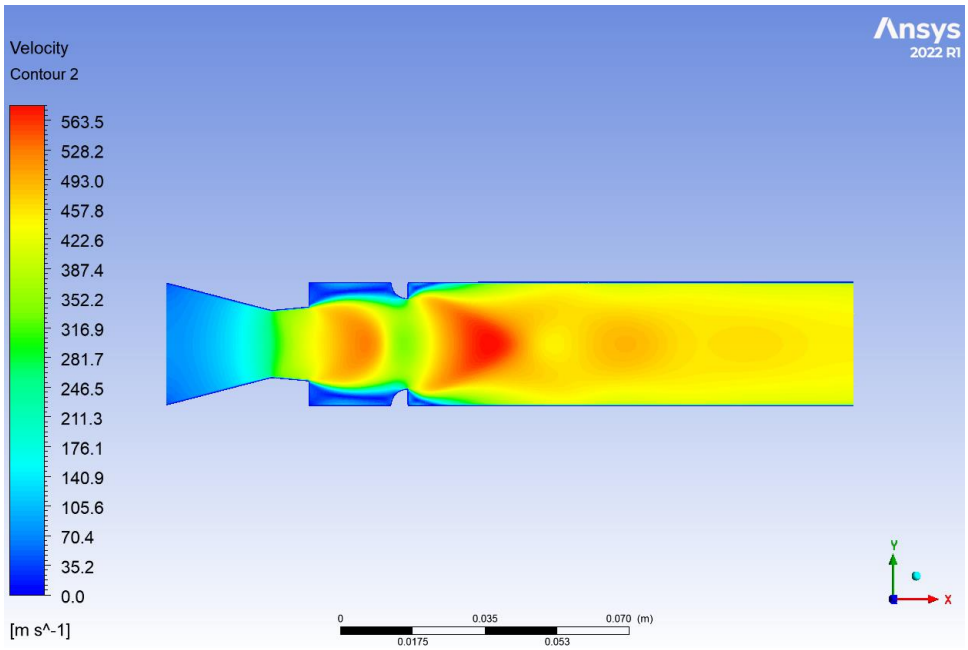

(b) Rib location 1D

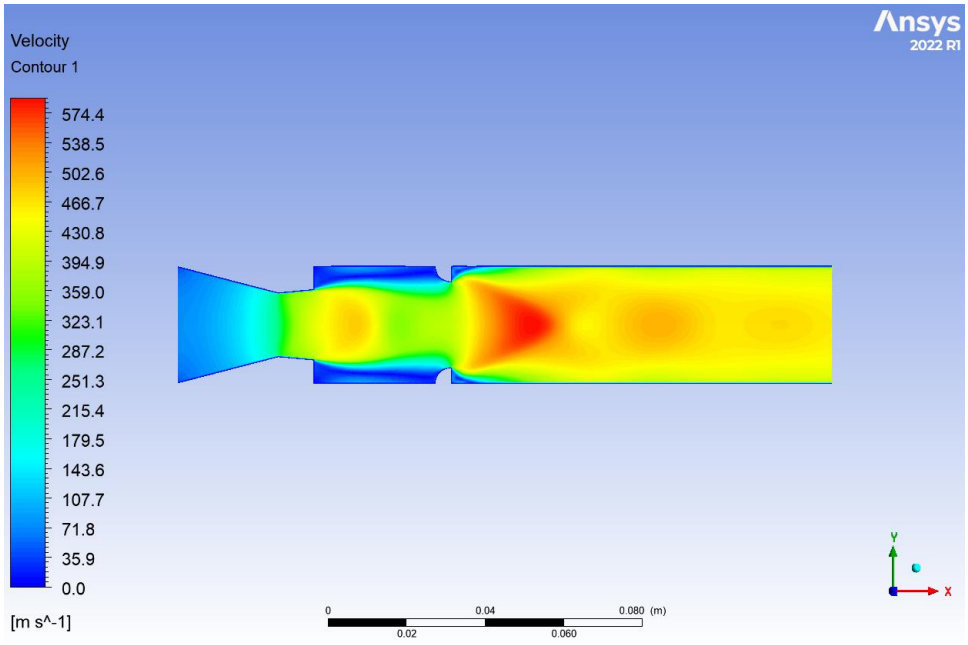

(c) Rib location 1.5D

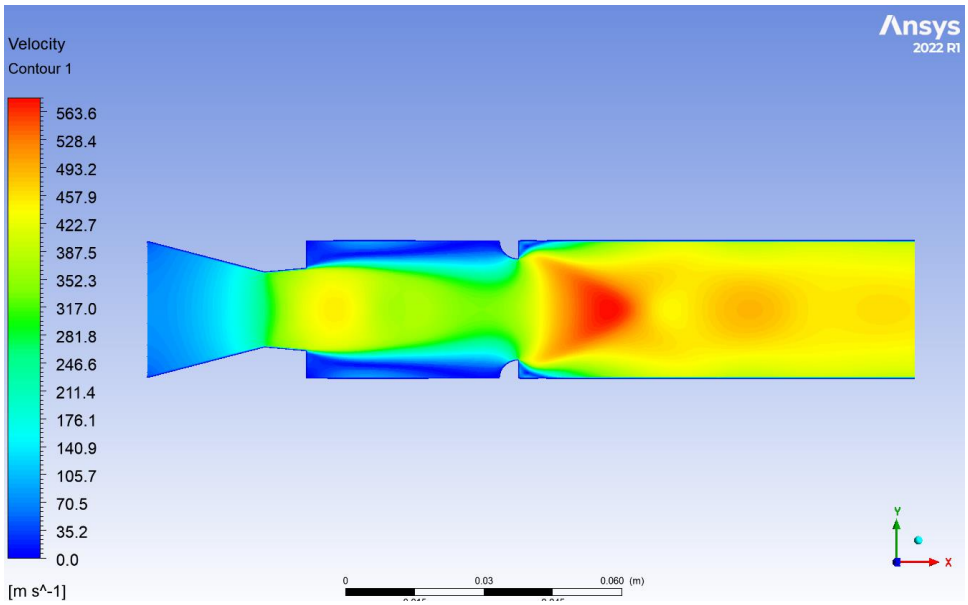

(d) Rib location 2D

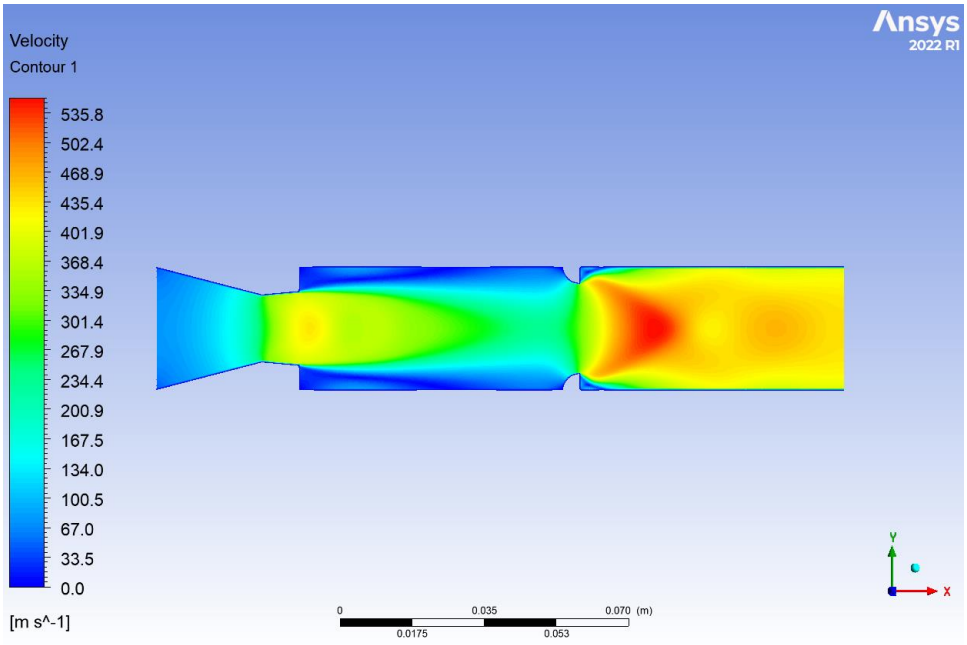

(e) Rib location 3D

Fig. 13. Velocity contours for rib diameter 4 mm, NPR=11, L/D ratio=6 and various rib locations

4.8 Velocity Streamlines for Rib Diameter 4 mm, NPR = 11, L/D Ratio = 6 and Various Rib Locations

Figure 14(a) to Figure 14(e) illustrate the velocity streamlines corresponding to a rib diameter of 4 mm, a Nozzle Pressure Ratio (NPR) of 11 and a Length-to-Diameter (L/D) ratio of 6. The streamlines are showcased for various rib placements within the duct (0.5D, 1D, 1.5D, 2D and 3D). However, this representation emphasizes the intricate fluid dynamics at play; the analysis reveals nuanced variations because the rib positioning significantly influences the flow characteristics.

Near nozzle ribs (0.5D, 1D) exhibit a limited impact on the reduction of recirculation; however, mid-duct ribs (1.5D, 2D) demonstrate a moderate enhancement in flow stability and base pressure. Downstream ribs (3D) yield maximum flow control, characterized by well-attached streamlines and minimal recirculation.

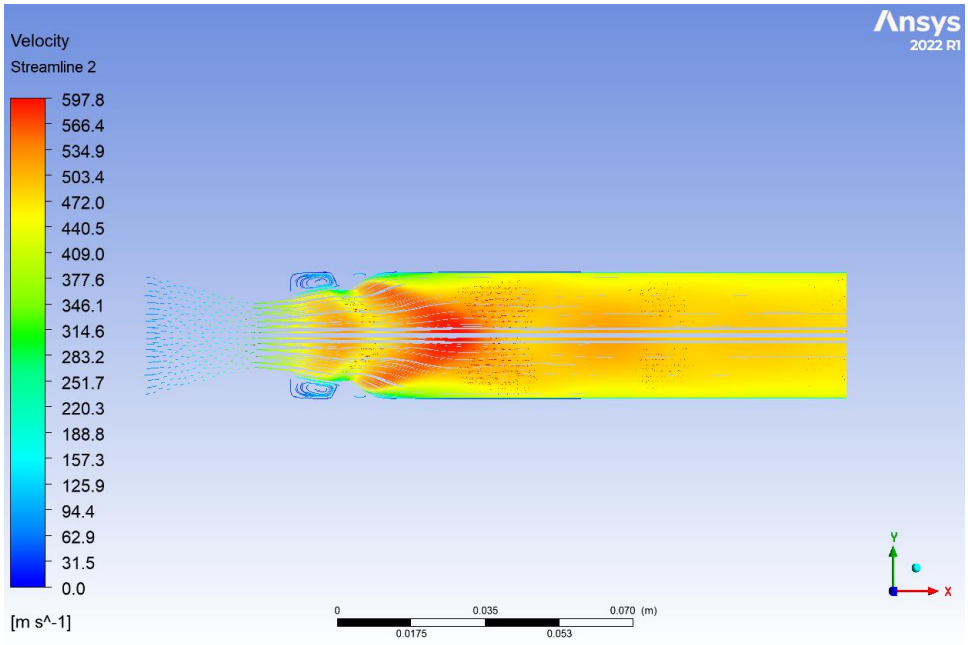

(a) Rib location 0.5D

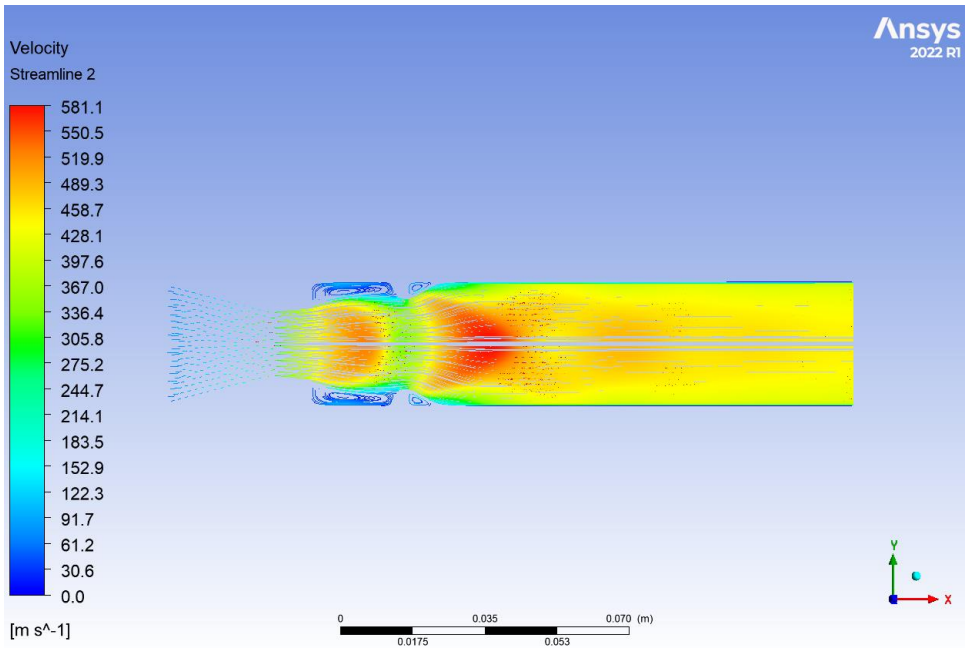

(b) Rib Location 1D

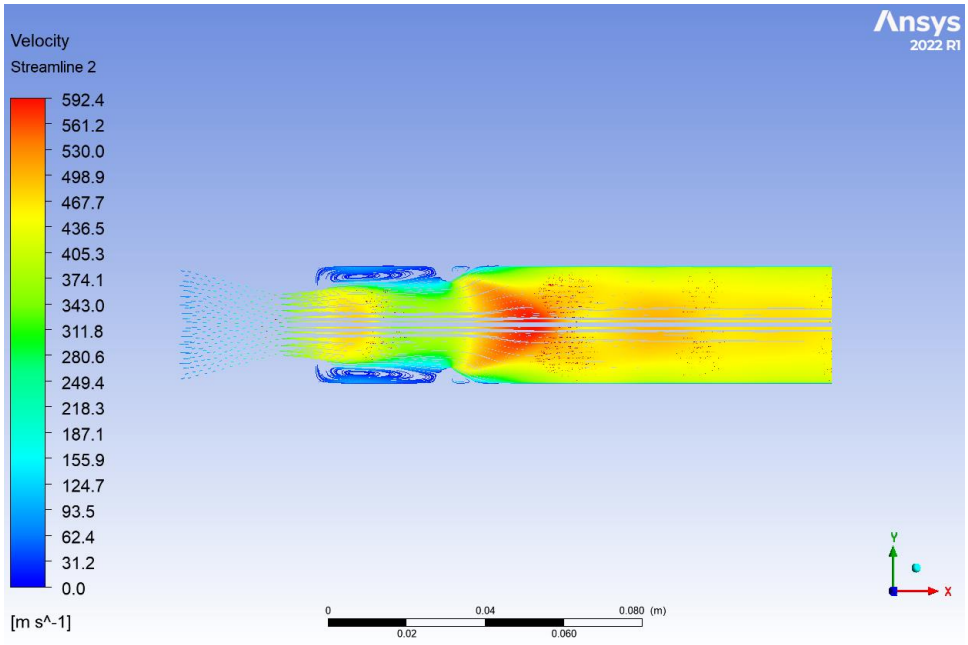

(c) Rib location 1.5D

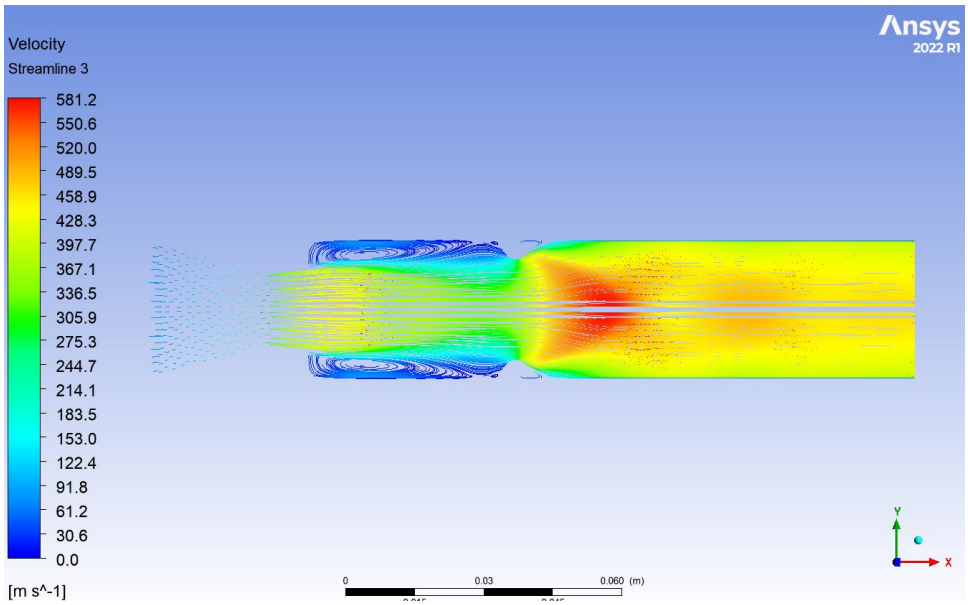

(d) Rib location 2D

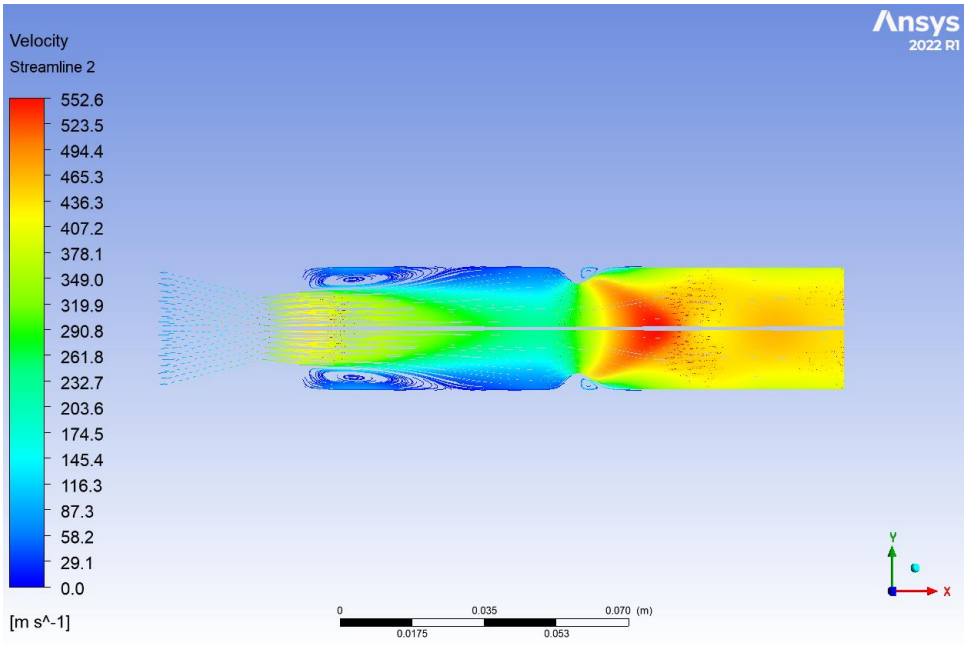

(e) Rib location 3D

Fig. 14. Velocity streamlines for rib diameter 4 mm, NPR=11, L/D ratio=6 and various rib locations

5. Conclusions

When a quarter rib as a control mechanism is placed at 11 mm from the base, all the ribs of radii ranging from 1 mm to 4 mm reduce the suction level in the separated recirculation zone. The base pressure ratio of 0.5 without control becomes 0.8, 1.2, 1.55 and 2 for NPR = 11 for various rib radii. There is a slight change in the base pressure ratios for various duct lengths ranging from 22 mm to 132 mm due to the impact of ambient atmospheric pressure. However, rib locations at 22 mm do not result in any appreciable change in the base pressure ratio. Instead, a rib with a 1 mm radius becomes inadequate and the outcomes of this study show that the base pressure ratio without control and with a 1 mm rib are identical. More so, the effectiveness of a rib with a 2 mm radius is marginally reduced. The effectiveness of 3 mm and 4 mm ribs as passive control remains identical, as was seen for rib placement at 11 mm. For rib placement at 33 mm, the results for those without ribs and those with 1 mm ribs are still the same as those in the previous case. However, there has been a considerable increase in the base pressure ratios and their values are 1.1. 1.8 and 2.6, barring minor changes at various duct lengths due to the impact of the back pressure. Similarly, when ribs are placed inside the duct at 44 mm, there is an increase in the base pressure ratio and its values are 1.25, 2 and 3. Similarly, for rib locations of 66 mm, these outcomes are more different again. Even a rib radius of 1 mm can considerably enhance the base pressure and those base pressure values are1.25, 1.3, 2.3 and 3.75. These results are technological demonstrations and the database created will help design and develop missiles, unguided rockets, artillery shells and aircraft bombs. It is also seen that even a tiny increase in base pressure will result in a considerable decrease in the base drag and, hence, an increase in the range of aerospace vehicles, leading to savings in fossil fuels and a reduction in global warming.

Acknowledgement
This research was not funded by any grant.

References

[1] Pathan, Khizar Ahmed, Syed Ashfaq, Prakash S. Dabeer and Sher Afgan Khan. "Analysis of parameters affecting thrust and base pressure in suddenly expanded flow from nozzle." (2019).

[2] Fiqri, Muhammad Ikhwan, Khizar Ahmed Pathan and Sher Afghan Khan. "Control of Suddenly Expanded Flow with Cavity at Sonic Mach Number." In *International Conference on Advances in heat Transfer and Fluid Dynamics*, pp. 3-15. Singapore: Springer Nature Singapore, 2022. https://doi.org/10.1007/978-981-99-7213-5_1

[3] Aqilah, Nur, Khizar Ahmed Pathan and Sher Afghan Khan. "Passive Control of Base Flow at Supersonic Mach Number for Area Ratio 4." In *International Conference on Advances in heat Transfer and Fluid Dynamics*, pp. 37-50. Singapore: Springer Nature Singapore, 2022. https://doi.org/10.1007/978-981-99-7213-5_4

[4] Pathan, Khizar A., Prakash S. Dabeer and Sher A. Khan. "Enlarge duct length optimization for suddenly expanded flows." *Advances in Aircraft and Spacecraft Science* 7, no. 3 (2020): 203-214.

[5] Pathan, Khizar Ahmed, Prakash S. Dabeer and Sher Afghan Khan. "Influence of expansion level on base pressure and reattachment length." *CFD Letters* 11, no. 5 (2019): 22-36.

[6] Azami, Muhammed Hanafi, Mohammed Faheem, Abdul Aabid, Imran Mokashi and Sher Afghan Khan. "Inspection of supersonic flows in a CD nozzle using experimental method." *International Journal of Recent Technology and Engineering* 8, no. 2S3 (2019): 996-999. https://doi.org/10.35940/ijrte.B1186.0782S319

[7] Pathan, Khizar Ahmed, Zakir Ilahi Chaudhary, Ajaj Rashid Attar, Sher Afghan Khan and Ambareen Khan. "Optimization of Nozzle Design for Weight Reduction using Variable Wall Thickness." *Journal of Advanced Research in Fluid Mechanics and Thermal Sciences* 112, no. 2 (2023): 86-101. https://doi.org/10.37934/arfmts.112.2.86101

[8] Azami, Muhammed Hanafi, Mohammed Faheem, Abdul Aabid, Imran Mokashi and Sher Afghan Khan. "Experimental research of wall pressure distribution and effect of micro jet at Mach 1.5." *International Journal of Recent Technology and Engineering* 8, no. 2S3 (2019): 1000-1003. https://doi.org/10.35940/ijrte.B1187.0782S319

[9] Khan, Sher Afghan, Abdul Aabid and Ahamed Saleel Chandu Veetil. "Influence of micro jets on the flow development in the enlarged duct at supersonic Mach number." *International Journal of Mechanical and Mechatronics Engineering* 19, no. 1 (2019): 70-82.

[10] Khan, Sher Afghan and E. Rathakrishnan. "Active control of suddenly expanded flows from underexpanded nozzles-Part II." *International Journal of Turbo and Jet Engines* 22, no. 3 (2005): 163-184. https://doi.org/10.1515/TJJ.2005.22.3.163

[11] Khan, Sher Afghan, M. A. Fatepurwala and K. N. Pathan. "CFD analysis of human powered submarine to minimize drag." *Ratio (L/D)* 4, no. 5 (2018).

[12] Pathan, Khizar A., Sher A. Khan, N. A. Shaikh, Arsalan A. Pathan and Shahnawaz A. Khan. "An investigation of boattail helmet to reduce drag." *Advances in Aircraft and Spacecraft Science* 8, no. 3 (2021): 239.

[13] Fakhruddin, Ahmad'Afy Ahmad, Fharukh Ahmed Ghasi Mahaboobali, Ambareen Khan, Mohammad Nishat Akhtar, Sher Afghan Khan and Khizar Ahmad Pathan. "Analysis of Base Pressure Control with Ribs at Mach 1.2 using CFD Method." *Journal of Advanced Research in Fluid Mechanics and Thermal Sciences* 123, no. 1 (2024): 108-143. https://doi.org/10.37934/arfmts.123.1.108143

[14] Khan, Ambareen, Parvathy Rajendran, Junior Sarjit Singh Sidhu, S. Thanigaiarasu, Vijayanandh Raja and Qasem Al-Mdallal. "Convolutional neural network modeling and response surface analysis of compressible flow at sonic and supersonic Mach numbers." *Alexandria Engineering Journal* 65 (2023): 997-1029. https://doi.org/10.1016/j.aej.2022.10.006

[15] Khan, Ambareen, Parvathy Rajendran, Junior Sarjit Singh Sidhu and Mohsen Sharifpur. "Experimental investigation of suddenly expanded flow at sonic and supersonic Mach numbers using semi-circular ribs: a comparative study between experimental, single layer, deep neural network (SLNN and DNN) models." *The European Physical Journal Plus* 138, no. 4 (2023): 314. https://doi.org/10.1140/epjp/s13360-023-03853-1

[16] Shaikh, Javed S., Krishna Kumar, Khizar A. Pathan and Sher A. Khan. "Analytical and computational analysis of pressure at the nose of a 2D wedge in high speed flow." *Advances in aircraft and spacecraft science* 9, no. 2 (2022): 119-130.

[17] Crasta, Asha, Khizer Ahmed Pathan and Sher Afghan Khan. "Numerical simulation of surface pressure of a wedge at supersonic Mach numbers and application of design of experiments." *Journal of advanced research in applied mechanics* 101, no. 1 (2023): 1-18. https://doi.org/10.37934/aram.101.1.118

[18] Crasta, Asha, Khizar Ahmed Pathan and Sher Afghan Khan. "Analytical and Numerical Simulation of Surface Pressure of an Oscillating Wedge at Hypersonic Mach Numbers and Application of Taguchi's Method." *Journal of Advanced Research in Applied Sciences and Engineering Technology* 30, no. 1 (2023): 15-30. https://doi.org/10.37934/araset.30.1.1530

[19] Shaikh, Javed Shoukat, Khizar Ahmed Pathan, Krishna Kumar and Sher Afghan Khan. "Effectiveness of Cone Angle on Surface Pressure Distribution along Slant Length of a Cone at Hypersonic Mach Numbers." *Journal of Advanced*

Research in Fluid Mechanics and Thermal Sciences 104, no. 1 (2023): 185-203. https://doi.org/10.37934/arfmts.104.1.185203

[20] Shaikh, Javed S., Krishna Kumar, Khizar A. Pathan and Sher A. Khan. "Computational analysis of surface pressure distribution over a 2d wedge in the supersonic and hypersonic flow regimes." *Fluid Dynamics & Materials Processing* 19, no. 6 (2023). https://doi.org/10.32604/fdmp.2023.025113

[21] Chaudhari, Pavan Bhaskar, Rachayya Arakerimath, Khizar Ahmed Pathan and Sher Afghan Khan. "Comparative Experimental Analysis and Performance Optimization of Single-Cylinder DI and HCCI Engine with Series Catalytic Converters." *Journal of Advanced Research in Fluid Mechanics and Thermal Sciences* 121, no. 1 (2024): 173-187. https://doi.org/10.37934/arfmts.121.1.173187

[22] Jain, Yogeshkumar, Vijay Kurkute, Sagar Mane Deshmukh, Khizar Ahmed Pathan, Ajaj Rashid Attar and Sher Afghan Khan. "The Influence of Plate Fin Heat Sink Orientation under Natural Convection on Thermal Performance: An Experimental and Numerical Study." *Journal of Advanced Research in Fluid Mechanics and Thermal Sciences* 114, no. 2 (2024): 118-129. https://doi.org/10.37934/arfmts.114.2.118129

[23] Khalil, Shaikh Sohel Mohd, Rai Sujit Nath Sahai, Nitin Parashram Gulhane, Khizar Ahmed Pathan, Ajaj Rashid Attar and Sher Afghan Khan. "Experimental Investigation of Local Nusselt Profile Dissemination to Augment Heat Transfer under Air Jet Infringements for Industrial Applications." *Journal of Advanced Research in Fluid Mechanics and Thermal Sciences* 112, no. 2 (2023): 161-173. https://doi.org/10.37934/arfmts.112.2.161173

[24] Shaikh, Sohel Khalil, Khizar Ahmed Pathan, Zakir Ilahi Chaudhary, B. G. Marlpalle and Sher Afghan Khan. "An investigation of three-way catalytic converter for various inlet cone angles using CFD." *CFD Letters* 12, no. 9 (2020): 76-90. https://doi.org/10.37934/cfdl.12.9.7690

[25] Shaikh, Sohel Khalil, Khizar Ahmed Pathan, Zakir Ilahi Chaudhary and Sher Afghan Khan. "CFD analysis of an automobile catalytic converter to obtain flow uniformity and to minimize pressure drop across the monolith." *CFD Letters* 12, no. 9 (2020): 116-128. https://doi.org/10.37934/cfdl.12.9.116128

[26] Kale, Dipak, Rachayya Arakerimath, Khizar Ahmed Pathan and Sher Afghan Khan. "Investigation on Water Erosion Behavior of Ti-based Metal Matrix Composite: Experimental Approach." *Journal of Advanced Research in Fluid Mechanics and Thermal Sciences* 122, no. 2 (2024): 71-82. https://doi.org/10.37934/arfmts.122.2.7182

[27] Sheikh, Fahim Rahim, Suresh Pandurang Deshmukh, Purushottam Ardhapurkar, Khizar Ahmed Pathan, Sohel Khalil Shaikh and Sher Afghan Khan. "Modeling and Experimental Validation of NePCM-Nanofluid-Based PVT System." *Journal of Advanced Research in Fluid Mechanics and Thermal Sciences* 122, no. 1 (2024): 205-222. https://doi.org/10.37934/arfmts.122.1.205222

[28] Khan, Ambareen, Abdul Aabid, Sher Afghan Khan, Mohammad Nishat Akhtar and Muneer Baig. "Comprehensive CFD analysis of base pressure control using quarter ribs in sudden expansion duct at sonic Mach numbers." *International Journal of Thermofluids* 24 (2024): 100908. https://doi.org/10.1016/j.ijft.2024.100908

[29] Khan, Ambareen, Sher Afghan Khan, Vijayanandh Raja, Abdul Aabid and Muneer Baig. "Effect of ribs in a suddenly expanded flow at sonic Mach number." *Heliyon* 10, no. 9 (2024). https://doi.org/10.1016/j.heliyon.2024.e30313

[30] Khan, Ambareen, Sher Afghan Khan, Mohammed Nishat Akhtar, Abdul Aabid and Muneer Baig. "Base Pressure Control with Semi-Circular Ribs at Critical Mach Number." *Fluid Dynamics & Materials Processing* 20, no. 9 (2024). https://doi.org/10.32604/fdmp.2024.049368

[31] Nurhanis, Tun, Ambareen Khan, Mohammad Nishat Akhtar and Sher Afghan Khan. "Control of Base Pressure at Supersonic Mach Number in a Suddenly Expanded Flow." *Journal of Advanced Research in Fluid Mechanics and Thermal Sciences* 109, no. 1 (2023): 210-225. https://doi.org/10.37934/arfmts.109.1.210225

[32] Khan, Ambareen, Nurul Musfirah Mazlan and Mohd Azmi Ismail. "Velocity Distribution and Base Pressure Analysis of Under Expanded Nozzle Flow at Mach 1.0." *Journal of Advanced Research in Fluid Mechanics and Thermal Sciences* 92, no. 1 (2022): 177-189. https://doi.org/10.37934/arfmts.92.1.177189

[33] Khan, Ambareen, Nurul Musfirah Mazlan and Ervin Sulaeman. "Effect of Ribs as Passive Control on Base Pressure at Sonic Mach Numbers." *CFD Letters* 14, no. 1 (2022): 140-151. https://doi.org/10.37934/cfdl.14.1.140151

[34] Khan, Ambareen, Mohd Azmi Ismail and Nurul Musfirah Mazlan. "Numerical Simulation of Suddenly Expanded Flow from Converging Nozzle at Sonic Mach Number." In *Proceedings of International Conference of Aerospace and Mechanical Engineering 2019: AeroMech 2019, 20–21 November 2019, Universiti Sains Malaysia, Malaysia*, pp. 349-359. Springer Singapore, 2020. https://doi.org/10.1007/978-981-15-4756-0_29

[35] Khan, Ambareen, Nurul Musfirah Mazlan and Mohd Azmi Ismail. "Analysis of flow through a convergent nozzle at Sonic Mach Number for Area Ratio 4." *Journal of Advanced Research in Fluid Mechanics and Thermal Sciences* 62, no. 1 (2019): 66-79.

[36] Khan, Ambareen, Nurul Musfirah Mazlan, Mohd Azmi Ismail and Mohammad Nishat Akhtar. "Experimental and numerical simulations at sonic and supersonic Mach numbers for area ratio 7.84." *CFD Letters* 11, no. 5 (2019): 50-60.

[37] Asadullah, Mohammed, Sher Afghan Khan, Waqar Asrar and E. Sulaeman. "Low-cost base drag reduction technique." *International Journal of Mechanical Engineering and Robotics Research* 7, no. 4 (2018): 428-432. https://doi.org/10.18178/ijmerr.7.4.428-432

[38] Rathakrishnan, E. "Effect of ribs on suddenly expanded flows." *AIAA journal* 39, no. 7 (2001): 1402-1404. https://doi.org/10.2514/2.1461